Nationaal Lucht- en Ruimtevaartlaboratorium
National Aerospace Laboratory NLR

Executive summary

Identification Of A Nonlinear Grey-Box Helicopter UAV Model

Problem area
We present a flight dynamics nonlinear model for a flybarless helicopter UAV, valid for a range of flight conditions, including the Vortex-Ring-State (VRS) and autorotation.

Description of work
To allow for computational efficiency, while maintaining a high-level of model fidelity, a grey-box modeling framework has been adopted, in which model uncertainty such as parameter uncertainties, unmodeled higher-order dynamics, and unmodeled static nonlinearities have been replaced by empirical coefficients. The derivation of these coefficients has been based upon a novel identification approach, anchored in the combined paradigms of nonlinear optimal control and neural networks.

Results and conclusions
Preliminary simulation results show that our model strategy is in good agreement with an equivalent FLIGHTLAB simulation model.

Applicability
Development of flight control systems for small-scale UAV helicopters.

Report no.
NLR-TP-2014-286

Author(s)
S. Taamallah

Report classification
UNCLASSIFIED

Date
July 2014

Knowledge area(s)
Helikoptertechnologie

Descriptor(s)
Unmanned Aerial Vehicle (UAV)
Helicopter Optimal Autorotation

This report is based on a presentation held at the AIAA Atmospheric Flight Mechanics Conference August 19 – 22, 2013, Boston, Massachusetts.

Nationaal Lucht- en Ruimtevaartlaboratorium, National Aerospace Laboratory NLR

Anthony Fokkerweg 2, 1059 CM Amsterdam,
P.O. Box 90502, 1006 BM Amsterdam, The Netherlands
Telephone +31 88 511 31 13, Fax +31 88 511 32 10, Web site: www.nlr.nl

Nationaal Lucht- en Ruimtevaartlaboratorium
National Aerospace Laboratory NLR

NLR-TP-2014-286

Identification Of A Nonlinear Grey-Box Helicopter UAV Model

S. Taamallah

This report is based on a presentation held at the AIAA Atmospheric Flight Mechanics Conference August 19 – 22, 2013, Boston, Massachusetts.

Customer	National Aerospace Laboratory NLR
Contract number	----
Owner	NLR
Division NLR	Aerospace Systems and Applications
Distribution	Unlimited
Classification of title	Unclassified
	July 2014

Approved by:

Author	Reviewer	Managing department
Date: 08/07/2014	Date: 11/7/2014	Date: 19/9/2014

Identification Of A Nonlinear Grey-Box Helicopter UAV Model

Skander Taamallah*†

National Aerospace Laboratory (NLR), 1059CM Amsterdam, The Netherlands

We present a flight dynamics nonlinear model for a flybarless helicopter UAV, valid for a range of flight conditions, including the Vortex-Ring-State (VRS) and autorotation. To allow for computational efficiency, while maintaining a high-level of model fidelity, a grey-box modeling framework has been adopted, in which model uncertainty such as parameter uncertainties, unmodeled higher-order dynamics, and unmodeled static nonlinearities have been replaced by empirical coefficients. The derivation of these coefficients has been based upon a novel identification approach, anchored in the combined paradigms of nonlinear optimal control and neural networks. Preliminary simulation results show that our model is in good agreement with an equivalent FLIGHTLAB model.

I. Introduction

In the past twenty years, scientific progress related to sensors technology and computational hardware has allowed for sustained research in the field of robotics. In particular, when considering flying robots, the availability of increasingly reliable, high performance, and miniaturized sensors, combined with advances in computing power on miniaturized hardware, has yielded impressive developments in the area of Unmanned Aerial Vehicles (UAVs)[a]. These unmanned vehicles have been developed for both civilian and military missions[b], while their *raison d'être* stems from the need for (real-time) information[c]. Further, UAV deployment and recovery from unprepared or confined sites may often be necessary, such as when operating from or above urban and natural canyons, forests, or naval ships. Hence, for these situations, a helicopter UAV capable of flying in and out of such restricted areas would represent a particularly attractive solution. Now, the development of such an autonomous helicopter system requires for an elaborate synergy between various engineering fields, including modeling, system identification, estimation and filtering, control, and finally software and hardware avionics integration. In this paper, we elaborate on the first and second items, i.e. the modeling and identification paradigms.

I.A. The Modeling Framework In Engineering

In the realm of physics and engineering, a wide range of systems may be subsumed as energy handling devices[2] that interact with inputs and outputs via energy ports. Understanding such systems is concomitant to the development of conceptual models, i.e. system models, which define both the system's structure and its associated behavior. Building such models requires selection between fundamentally different design philosophies, namely (i) mechanistic/first-principles, also called White-Box (WB) vs. empirical-based, known as Black-Box (BB), or even a mixture of both resulting in a Grey-Box (GB) representation,[3] and (ii) Linear

*R&D Engineer, Aircraft Systems Department, National Aerospace Laboratory (NLR), 1059CM Amsterdam, The Netherlands.

†Ph.D. Student, Delft Center for Systems and Control (DCSC), Faculty of Mechanical, Maritime and Materials Engineering, Delft University of Technology, 2628CD Delft, The Netherlands.

[a]Although industry and the regulators have now adopted Unmanned Aerial System (UAS) as the preferred term for Unmanned Aircraft, as UAS encompasses all aspects of deploying these vehicles and not just the platform itself.

[b]UAVs have typically been associated with the so-called *DDD* tasks:[1] Dull e.g. long duration, Dirty e.g. sampling for hazardous materials, and Dangerous e.g. extreme exposure to hostile action.

[c]Spanning a broad spectrum, i.e. visual, electromagnetic, physical, nuclear, biological, chemical, or meteorological information.

Time-Invariant (LTI) vs. NonLinear and/or Time-Varying (NL-TV), or again a mixture of both resulting in a State-Dependent Riccati Equation (SDRE), Gain Scheduling (GS), or Linear Parameter Varying (LPV) description.

I.A.1. White- vs. Black-Box Modeling

White-Box models refer to modeling structures based upon detailed understandings of the underlying physical laws governing the system, hence providing substantial contribution towards behavior recognition from a scientific viewpoint. On the other hand, when a thorough understanding of the system's laws is not required or necessary, then BB model structures, derived from specific observations, result in simpler representations, with the additional advantage of shorter design and development cycles.[3] When used independently, both of these approaches may, at times, be unattractive. For instance, in the case of a WB representation, and when the system's first-principles laws are only partially understood, the development of such a WB model may become a challenging task, and further result in a final product with questionable model fidelity. Alternatively, even when the laws of physics happen to be well comprehended, the development and validation of such WB models may turn out to be highly resource demanding, especially in the case of complex and high-order industrial plants, such as helicopters. Next, one also has to consider the intended model application, since this latter may as well impose restrictions on the modeling structure and its complexity. For example, depicting a system with an accurate mathematical representation, in a computationally tractable way for its intended application, may result in conflicting requirements.[4]

On the other hand, for the case of BB models, their development may be impaired by the well-known principle of induction[d] deficiencies. Indeed it is conspicuously accepted that induction has serious endemic limitations, as a finite number of observations is generally not sufficient to envelop the infinite number of model operating regimes[e].[3,5]

I.A.2. Grey-Box Modeling

Consequently, and for some practical applications, it is the appropriate mixing of mechanistic with empirical knowledge that allows to leverage, in a reciprocal way, the drawbacks of one method with the benefits of the other. By so doing we create the so-called GB modeling paradigm, also known as hybrid modeling.[6] For instance, in a mainly WB approach, aspects of the system that are not sufficiently well understood, which in general are regrouped under the umbrella of modeling uncertainties (i.e. unmodeled higher-order dynamics, unmodeled static nonlinearities, parametric uncertainties, and delays) may be described by a BB model, this latter being identified through parameter estimation techniques based upon experimental data. Conversely, in a predominantly BB approach, some physical insight may often be instrumental to make certain structural choices, such as the adequate model order and the nature of its nonlinearities.[3] In this context, the GB modeling meets (i) the required end-product accuracy and reliability, (ii) the computational tractability specifications, and (iii) the development cost limits, all of which have resulted in a growing interest towards the GB modeling structure, imbued by the increasing demand for nonlinear models to be applied in intelligent and autonomous systems and vehicles, and various optimization based disciplines.

I.B. Our Grey-Box Helicopter Model

The purpose of this paper is to present a novel, highly accurate, computationally efficient, GB helicopter UAV model, suitable for optimal trajectories computation.[7,8] While the WB model is loosely based on the ideas we presented in Ref. 9, the derivation of the BB model is based upon a novel identification approach, anchored in the combined paradigms of nonlinear optimal control and neural networks.

Now with regard to the WB representation, it has been tailored towards small-scale flybarless[f] helicopter UAVs, and is also valid for a range of flight conditions including the Vortex-Ring-State (VRS) and autorotation. The nonlinear dynamics includes the twelve-states rigid body equations of motion, the single-state

[d] The principle of induction suggests that it is possible to generalize from a sufficiently large number of consistent observations.[3,5]

[e] The region for which the model is locally valid is called an operating regime.

[f] Without a Bell-Hiller stabilizing bar.

main rotor Revolutions Per Minute (RPM), a static Tip-Path-Plane (TPP) main rotor model, and a static uniform main rotor inflow model. Besides, the model accommodates for flight in the VRS, and for deterministic wind and Dryden stochastic atmospheric turbulence. Further, static ground effect has been accounted for by a correction factor applied to the non-dimensional total velocity at the rotor disk center. The fuselage model is based upon aerodynamic lift and drag coefficients, which are tabulated as a function of airflow angle of attack and sideslip angles. These lookup tables are derived from a scaled-down full-size helicopter fuselage aerodynamic model. The horizontal and vertical tails are based upon flat plate models, whereas the tail rotor has been modeled as a Bailey type rotor. Finally the paper reviews all assumptions made in deriving the model, i.e. structural, aerodynamics, and dynamical simplifications, which are valid for stability and control investigations of helicopters up to an advance ratio limit[g] of about 0.3.[10–12]

II. White-Box Modeling

II.A. Rigid Body Equations of Motion

II.A.1. Assumptions

- The vehicle has a longitudinal plane of symmetry, and has constant mass, inertia, and Center of Gravity (CG) position, hence fuel consumption and/or payload pickup/release are neglected. The vehicle is also a rigid system, i.e. it does not contain any flexible structures, hence the time derivative of the inertia matrix is zero. Further variations of helicopter CG locations due to main rotor blades position are neglected.
- The vehicle height above ground is very small compared to the earth radius, implying a gravitation independent of height and thus constant. Additionally the center of mass and CG are identical for a constant gravity field.
- The earth is assumed fixed and flat. There is then no longer a distinction between the directions of gravitational force and the force of gravity, hence the external force becomes the force of gravity[h]. Gravity is also a function of latitude, for all practical purpose we will consider the medium latitudes of 52°.
- Finally, we neglect the effect of buoyancy or Armichedes force, which is negligible with respect to all other forces.

II.A.2. Modeling

To start, our model is defined by a thirteen-state vector, and a four-control input vector

$$\begin{aligned}\mathbf{x} &= \begin{pmatrix} x_N & x_E & x_Z & \phi & \theta & \psi & u & v & w & p & q & r & \Omega_{MR} \end{pmatrix}^T \\ \mathbf{u} &= \begin{pmatrix} \theta_0 & \theta_{TR} & \theta_{1c} & \theta_{1s} \end{pmatrix}^T \end{aligned} \tag{1}$$

Then, classical Newtonian mechanics and the fundamental relationship of kinematics provide us with the standard twelve-state rigid body equations of motion, following notations of Ref. 13.

$$\begin{pmatrix} \dot{x}_N \\ \dot{x}_E \\ \dot{x}_Z \end{pmatrix}^o = \begin{pmatrix} V_N \\ V_E \\ V_Z \end{pmatrix}^o \qquad \begin{pmatrix} V_N \\ V_E \\ V_Z \end{pmatrix}^o = \mathbb{T}_{ob}. \begin{pmatrix} u \\ v \\ w \end{pmatrix}^b \tag{2}$$

$$\begin{pmatrix} \dot{u} \\ \dot{v} \\ \dot{w} \end{pmatrix}^b = - \begin{pmatrix} q.w - r.v \\ r.u - p.w \\ p.v - q.u \end{pmatrix}^b + g. \begin{pmatrix} -\sin\theta \\ \cos\theta \sin\phi \\ \cos\theta \cos\phi \end{pmatrix}^b + \frac{\mathbf{F}_{aero,G_{Fus}}}{m_{Fus}}^b \tag{3}$$

[g] The flight envelope of small-scale helicopters is well within this limit.
[h] For further details on the geoid earth and gravity see Ref. 13, 14.

$$\begin{pmatrix} \dot{p} \\ \dot{q} \\ \dot{r} \end{pmatrix}^b = \mathbb{I}_{Fus}^{-1}.\left(\mathbf{M}^b_{G_{Fus}} - \begin{pmatrix} p \\ q \\ r \end{pmatrix}^b \times \left(\mathbb{I}_{Fus}.\begin{pmatrix} p \\ q \\ r \end{pmatrix}^b\right)\right) \tag{4}$$

$$\begin{pmatrix} \dot{\phi} \\ \dot{\theta} \\ \dot{\psi} \end{pmatrix}^b = \begin{bmatrix} 1 & \sin\theta.\frac{\sin\phi}{\cos\theta} & \sin\theta.\frac{\cos\phi}{\cos\theta} \\ 0 & \cos\phi & -\sin\phi \\ 0 & \frac{\sin\phi}{\cos\theta} & \frac{\cos\phi}{\cos\theta} \end{bmatrix}.\begin{pmatrix} p \\ q \\ r \end{pmatrix}^b \tag{5}$$

$$\mathbb{T}_{ob} = \begin{bmatrix} \cos\theta\cos\psi & \sin\theta\sin\phi\cos\psi - \sin\psi\cos\phi & \cos\psi\sin\theta\cos\phi + \sin\phi\sin\psi \\ \sin\psi\cos\theta & \sin\theta\sin\phi\sin\psi + \cos\psi\cos\phi & \sin\theta\cos\phi\sin\psi - \sin\phi\cos\psi \\ -\sin\theta & \cos\theta\sin\phi & \cos\theta\cos\phi \end{bmatrix} \tag{6}$$

With $\mathbf{F}^b_{aero,G_{Fus}}$ the aerodynamic forces experienced by the fuselage CG in the body frame F_b, and $\mathbf{M}^b_{G_{Fus}}$ the moments of all forces expressed at the fuselage[i] CG in frame F_b.

These total forces include contributions from the main rotor, tail rotor, fuselage, vertical tail, and horizontal tail, and are given by

$$\begin{aligned}\mathbf{F}^b_{aero,G_{Fus}} = \begin{pmatrix} F_{Xaero,G_{Fus}} \\ F_{Yaero,G_{Fus}} \\ F_{Zaero,G_{Fus}} \end{pmatrix}^b = ... \\ \begin{pmatrix} F_{x_{MR}} \\ F_{y_{MR}} \\ F_{z_{MR}} \end{pmatrix}^b + \begin{pmatrix} F_{x_{TR}} \\ F_{y_{TR}} \\ F_{z_{TR}} \end{pmatrix}^b + \begin{pmatrix} F_{x_F} \\ F_{y_F} \\ F_{z_F} \end{pmatrix}^b + \begin{pmatrix} F_{x_{VT}} \\ F_{y_{VT}} \\ F_{z_{VT}} \end{pmatrix}^b + \begin{pmatrix} F_{x_{HT}} \\ F_{y_{HT}} \\ F_{z_{HT}} \end{pmatrix}^b + \begin{pmatrix} \Theta_{Fx} \\ \Theta_{Fy} \\ \Theta_{Fz} \end{pmatrix}\end{aligned} \tag{7}$$

with $(\Theta_{Fx}\ \Theta_{Fy}\ \Theta_{Fz})^T$ a vector of empirical coefficients, which will be addressed in Section III. The total moments, which also include the components due to the non-collocation of the vehicle CG and fuselage CG, are given by

$$\begin{aligned}\mathbf{M}^b_{G_{Fus}} = \begin{pmatrix} M_{X,G_{Fus}} \\ M_{Y,G_{Fus}} \\ M_{Z,G_{Fus}} \end{pmatrix}^b = \begin{pmatrix} M_{x_{MR}} \\ M_{y_{MR}} \\ M_{z_{MR}} \end{pmatrix}^b + \begin{pmatrix} M_{x_{TR}} \\ M_{y_{TR}} \\ M_{z_{TR}} \end{pmatrix}^b + \begin{pmatrix} M_{x_F} \\ M_{y_F} \\ M_{z_F} \end{pmatrix}^b + \begin{pmatrix} M_{x_{VT}} \\ M_{y_{VT}} \\ M_{z_{VT}} \end{pmatrix}^b + \begin{pmatrix} M_{x_{HT}} \\ M_{y_{HT}} \\ M_{z_{HT}} \end{pmatrix}^b \\ + \begin{pmatrix} -y_F.F_{Zaero,G_{Fus}} + z_F.F_{Yaero,G_{Fus}} \\ -z_F.F_{Xaero,G_{Fus}} + x_F.F_{Zaero,G_{Fus}} \\ -x_F.F_{Yaero,G_{Fus}} + y_F.F_{Xaero,G_{Fus}} \end{pmatrix}^b + \begin{pmatrix} \Theta_{Mx} \\ \Theta_{My} \\ \Theta_{Mz} \end{pmatrix}\end{aligned} \tag{8}$$

with again $(\Theta_{Mx}\ \Theta_{My}\ \Theta_{Mz})^T$ a vector of empirical coefficients, which will be addressed in Section III. The derivation of the here-above presented forces and moments is given in the next sections.

[i] Note that fuselage inertia and fuselage CG are used here rather than vehicle inertia and vehicle CG, since in the moments term $\mathbf{M}^b_{G_{Fus}}$ we have already accounted for rotor moments due to main rotor inertial loads.

II.B. Main Rotor Modeling

II.B.1. Assumptions

Structural Simplifications

- Rotor shaft forward and lateral tilt-angles are zero. The blade has zero twist, constant chord, zero sweep, constant thickness ratio, and a uniform mass distribution.
- Rigid rotor blade in bending. Neglecting higher modes (harmonics), since higher modes are only pronounced at high speed.[15,16] Further, blade torsion is neglected since small-scale helicopter blades are generally relatively stiff.
- Rotor inertia inboard of the flap hinge is assumed small and thus neglected.

Aerodynamics Simplifications

- Vehicle flies at a low altitude, hence neglecting air density and temperature variations. Blade element theory[j] is used to compute rotor lift and drag forces. Radial flow along blade span is ignored. Pitch, lag, and flap angles are assumed to be small.
- Momentum theory[k] is used to compute the uniform inflow component.
- Compressibility effects are disregarded, which is a reasonable assumption considering small-scale helicopter flight characteristics. Viscous flow effects are also disregarded, which is a valid assumption for low angle of attacks and un-separated flow.[19,20]
- Aerodynamic interference effects between the main rotor and other helicopter modules, e.g. fuselage or tail rotor, are neglected.
- When deriving an expression for the main rotor torque (i.e. yaw moment), only a vertical flight inflow and power component is considered, hence omitting forward flight contributions.
- The presence of the fuselage just under the main rotor acts as a so-called pseudo-ground effect, resulting in some thrust recovery. This phenomenon is neglected in our paper, although an estimate of its effect may be obtained from Ref. 21.

Dynamical Simplifications

- Dynamic twist[l] is neglected. Hence blade CG is assumed to be located on the blade section quarter chord line.
- Unsteady (frequency dependent) effect for time-dependent development of blade lift and pitching moment, due to changes in local incidence are ignored. For example dynamic stall, due to rapid pitch changes, is ignored.
- A balanced rotor is assumed. In general most of the inertial terms, contributing to main rotor moments, vanish[m] when integrated around 2π azimuth.

[j] Calculates the forces on the blade due to its motion through the air. It is assumed that each blade section acts as a 2-D airfoil to produce aerodynamic forces, with the influence of the wake contained in an induced angle of attack at the blade section.[17]

[k] States that the total force acting on a control volume is equal to the rate of change of momentum, i.e. mass flow entering and leaving this control volume.[17,18]

[l] Any offset in blade chordwise CG or aerodynamic center position will result in a coupling of the flap and torsion Degrees Of Freedom (DOF) in blade elastic modes.[15]

[m] These terms should be retained when evaluating rotor out-of-balance loads.[22]

II.B.2. Modeling

VELOCITIES The main rotor hub aerodynamic velocity in the body frame F_b is given by

$$\mathbf{V}^b_{a,MR} = \begin{pmatrix} V_{a,MR_u} \\ V_{a,MR_v} \\ V_{a,MR_w} \end{pmatrix}^b = \begin{pmatrix} u + (q - q_w).z_H - (r - r_w).y_H \\ v - (p - p_w).z_H + (r - r_w).x_H \\ w + (p - p_w).y_H - (q - q_w).x_H \end{pmatrix}^b - \begin{pmatrix} u_w \\ v_w \\ w_w \end{pmatrix}^b \tag{9}$$

With

$$\begin{pmatrix} u_w \\ v_w \\ w_w \end{pmatrix}^b = \mathbb{T}_{bo}. \begin{pmatrix} u_w \\ v_w \\ w_w \end{pmatrix}^o \quad \text{and} \quad \mathbb{T}_{bo} = \mathbb{T}^{-1}_{ob} \tag{10}$$

And the non-dimensional velocities are expressed as follows

$$\mu_x = -V_{a,MR_u}/V_{MRref} \tag{11a}$$
$$\mu_y = -V_{a,MR_v}/V_{MRref} \tag{11b}$$
$$\mu_z = -V_{a,MR_w}/V_{MRref} \tag{11c}$$
$$\mu_{xy} = \sqrt{\mu_x^2 + \mu_y^2} \quad \text{and} \quad V_{MRref} = \Omega_{MR}.R_{rot} \tag{11d}$$

INFLOW As for the inflow, we consider only the uniform component and we neglect inflow dynamics. Our model is a simplified implementation of the expressions presented in Ref. 23, 24, with the inclusion of the VRS correction from Ref. 25. The momentum theory induced flow λ_m is given from Ref. 17

$$\lambda_m^2.\Big[(\lambda_m + \mu_z)^2 + \mu_{xy}^2\Big] = \left(\frac{v_h}{V_{MRref}}\right)^4 \quad \text{if} \quad \mu_z \geq 0 \quad \text{or} \quad \mu_z.\frac{V_{MRref}}{v_h} \leq -2 \tag{12}$$

In the VRS, it is given from Ref. 25

$$\lambda_m^2.\Big[(\lambda_m + \mu_z)^2 + \mu_{xy}^2 + \left(\frac{v_h}{V_{MRref}}\right)^2.f(\mu_{xy}^-).g(\bar{\lambda})\Big] = \left(\frac{v_h}{V_{MRref}}\right)^4 \quad \text{if} \quad \mu_z.\frac{V_{MRref}}{v_h} \in [-2, 0] \tag{13}$$

In the static case, also from Ref. 23, 24, the rotor uniform induced velocity, normal to the TPP, is given by

$$v_{i_o} = G_{eff}/(2V_T).(-C_T^{TPP}).V_{MRref} \tag{14}$$

Where C_T^{TPP} is the main rotor thrust coefficient in the TPP frame. Since the TPP angles are assumed small, we conjecture that it is also valid in the Hub-Body frame, i.e. $C_T^{HB} \simeq C_T^{TPP}$. Now, from Ref. 17 we get, after rearranging terms, the thrust coefficient in the Hub-Body frame

$$\begin{aligned} C_T^{HB} &= A + B.v_{i_o} \quad \text{with} \\ A &= -0.5.\sigma_{MR}.CL_{MR_\alpha}.\theta_0/3.(B^3 + 1.5B.\mu_{xy}^2) \\ &\quad -0.25.\sigma_{MR}.CL_{MR_\alpha}.B^2.\Big(V_{a,MR_w}/V_{MRref} + \mu_{xy}.(\beta_{1c} + \theta_{1s})\Big) \\ B &= 0.25.\sigma_{MR}.CL_{MR_\alpha}.B^2/V_{MRref} \end{aligned} \tag{15}$$

And V_T gives the total flow,[25] through the rotor disk, as

$$V_T = \sqrt{(\lambda_m + \mu_z)^2 + \mu_{xy}^2 + (v_h/V_{MRref})^2.f(\bar{\mu_{xy}}).g(\bar{\lambda})} \tag{16}$$

With the following correction factors

$$\begin{array}{ll} f(\bar{\mu_{xy}}) & = 1 - 2.\bar{\mu_{xy}}^2 \quad \text{if} \quad \bar{\mu_{xy}} \in [0, 0.707] \\ f(\bar{\mu_{xy}}) & = 0 \quad \text{otherwise} \\ g(\bar{\lambda}) & = \frac{1}{(2+\bar{\lambda})^2} - \bar{\lambda}^2 + (1+\bar{\lambda}).\Big[0.109 + 0.217(\bar{\lambda} - 0.15)^2\Big] \quad \text{if} \quad \bar{\lambda} \in [-1, 0.6378] \\ g(\bar{\lambda}) & = 0 \quad \text{otherwise} \\ \bar{\lambda} & = (\lambda_m + \mu_z)/(v_h/V_{MRref}) \\ \bar{\mu_{xy}} & = \mu_{xy}/(v_h/V_{MRref}) \end{array} \tag{17}$$

From Eq (14) - Eq (15), we can now derive an approximated and simplified expression for the static uniform inflow, in which we have assumed the longitudinal rotor TPP tilt angle to be small $\beta_{1c} \simeq 0$, we get

$$\begin{array}{ll} v_{i_o} & = A.C/(1 - B.C) \\ C & = -G_{eff}/(2V_T).V_{MRref} \end{array} \tag{18}$$

Finally, the ground effect correction factor is given from Ref. 26 as

$$G_{eff} = \frac{1}{0.9926 + 0.0379(2R_{rot}/h_H)^2} \tag{19}$$

Tip-Path-Plane (TPP) Angles As for the Tip-Path-Plane (TPP) model, here too we assume a static behavior. The model is a simplified[n] implementation of the expressions presented in Ref. 11,12. In particular we neglect the effect of roll, pitch and vertical accelerations on the rotor TPP angles.

$$\begin{pmatrix} \beta_0 \\ -\beta_{1c} \\ -\beta_{1s} \end{pmatrix} = \mathbb{K}^{-1}.\left(\mathbb{F}_\theta.\begin{pmatrix} \theta_0 \\ -\theta_{1c} \\ -\theta_{1s} \end{pmatrix} + \mathbb{F}_{pq}.\begin{pmatrix} p \\ q \end{pmatrix} + \lambda.\mathbb{F}_\lambda + \mathbb{F}_0\right) \tag{20}$$

With the rotor total inflow expressed by

$$\lambda = (-V_{a,MR_w} + v_{i_o})/V_{MRref} \tag{21}$$

And the matrices $\mathbb{K}$, $\mathbb{F}_\theta$, $\mathbb{F}_{pq}$, $\mathbb{F}_\lambda$, and $\mathbb{F}_0$ given by

$$\mathbb{K} = \Omega_{MR}^2.\begin{bmatrix} P^2 & F_1.\mu_{xy} & 0 \\ F_2.\mu_{xy} & P^2 - 1 & G_1 \\ 0 & -G_1 & P^2 - 1 \end{bmatrix} \tag{22}$$

[n] We do not use the wind-axis formalism of Ref. 11, 12

$$\mathbb{F}_\theta = \Omega_{MR}^2 . \begin{bmatrix} G_2 & 0 & F_2.\mu_{xy} \\ 0 & G_2 & 0 \\ F_2.\mu_{xy} & 0 & G_2 \end{bmatrix} \tag{23}$$

Where we modified the element $\mathbb{F}_\theta(3,1)$, in Eq (23) compared to Ref. 11,12, since this gives better results. The remaining matrices are given by

$$\mathbb{F}_{pq} = \Omega_{MR} . \begin{bmatrix} -F_3.\mu_{xy} & 0 \\ H_1 & -H_2 \\ H_2 & H_1 \end{bmatrix} \tag{24}$$

$$\mathbb{F}_\lambda = \Omega_{MR}^2 . \begin{pmatrix} G_3 \\ 0 \\ F_4.\mu_{xy} \end{pmatrix} \tag{25}$$

$$\mathbb{F}_0 = \begin{pmatrix} -C_0/I_b.g \\ 0 \\ 0 \end{pmatrix} \tag{26}$$

With

$$P^2 = 1 + K_{S_\beta}/(I_b.\Omega_{MR}^2) + \Delta_e/I_b.C_0 \tag{27a}$$
$$F_1 = -\epsilon/8.\gamma \tag{27b}$$
$$F_2 = -1/2(1/3 - \epsilon/2).\gamma \tag{27c}$$
$$F_3 = 1/8(2/3 - \epsilon).\gamma \tag{27d}$$
$$F_4 = -1/2(1/2 - \epsilon).\gamma \tag{27e}$$
$$G_1 = 1/2(1/4 - 2/3\epsilon).\gamma \tag{27f}$$
$$G_2 = 1/2(1/4 - 1/3\epsilon).\gamma \tag{27g}$$
$$G_3 = 1/2(1/3 - 1/2\epsilon).\gamma \tag{27h}$$
$$H_1 = 2(1 + \Delta_e/I_b.C_0) \tag{27i}$$
$$H_2 = 1/2(1/4 - 1/3.\epsilon).\gamma \tag{27j}$$

FORCES The rotor force coefficients, in the Hub-Body wind-axis frame F_{HBw} are given in Ref. 17. We did not use the side-force coefficient from Ref. 17 since it did not provide satisfactory results (when our model was compared with an equivalent FLIGHTLAB® model). For the drag, and thrust coefficients we have

$$C_{H_{MR}}^{HBw} = \frac{\sigma_{MR}.CD_{MR}}{8}.\left(3\mu_{xy} + 1.98\mu_{xy}^{2.7}\right) + \frac{\sigma_{MR}.CL_{MR_\alpha}}{2}.\left(\frac{\theta_0}{2}.\mu_{xy}.\lambda - \frac{\theta_{1c}.\beta_0}{6} + \frac{\theta_{1s}}{4}.\lambda + \frac{\mu_{xy}.\beta_0^2}{4}\right) \tag{28}$$

$$C_{T_{MR}}^{HBw} = -\frac{\sigma_{MR}.CL_{MR_\alpha}}{2}.\left(\frac{\theta_0}{3}.\left[B^3 + \frac{3}{2}B.\mu_{xy}^2\right] - \frac{B^2}{2}.\left[\lambda - \mu_{xy}.(\beta_{1c} + \theta_{1s})\right]\right) \tag{29}$$

Which gives in the body frame F_b

$$\begin{pmatrix} C_{HMR} \\ C_{YMR} \\ C_{TMR} \end{pmatrix}^{b} = \mathbb{T}_{b(HBw)} \cdot \begin{pmatrix} C_{HMR} \\ 0 \\ C_{TMR} \end{pmatrix}^{HBw} \tag{30}$$

With

$$\mathbb{T}_{b(HBw)} = \mathbb{T}_{b(HB)} . \mathbb{T}_{HB(HBw)} \tag{31}$$

Now since the main rotor shaft tilt angle is zero, the Hub-Body frame F_{HB} and the vehicle body frame F_b are identical, i.e. $\mathbb{T}_{b(HB)} = \mathbb{I}$. And

$$\mathbb{T}_{(HB)(HBw)} = \begin{bmatrix} -\cos\beta_{MR} & -\sin\beta_{MR} & 0 \\ -\sin\beta_{MR} & \cos\beta_{MR} & 0 \\ 0 & 0 & 1 \end{bmatrix} \tag{32}$$

The main rotor sideslip angle is expressed from the fuselage sideslip angle Eq (54) as

$$\beta_{MR} = \mod(\beta_F, 2\pi) \tag{33}$$

Finally expressing the main rotor forces in the body frame we get

$$\begin{pmatrix} F_{x_{MR}} \\ F_{y_{MR}} \\ F_{z_{MR}} \end{pmatrix}^{b} = \begin{pmatrix} C_{HMR} \\ C_{YMR} \\ C_{TMR} \end{pmatrix}^{b} . \rho . \pi . R_{rot}^2 . V_{MRref}^2 \tag{34}$$

Moments The roll and pitch moments due to the flap hinge spring are given as in Ref. 17

$$L^b_{(MR,flap)} = -\frac{1}{1-\frac{\Delta_e}{R_{rot}}} . \frac{N_b}{2} . K_{S_\beta} . \Gamma . \beta_{1s} \tag{35a}$$

$$M^b_{(MR,flap)} = -\frac{1}{1-\frac{\Delta_e}{R_{rot}}} . \frac{N_b}{2} . K_{S_\beta} . \beta_{1c} \tag{35b}$$

The inertia roll and pitch moments, which arise when the plane of a rotor with offset hinges is tilted relative to the shaft, are given as in Ref. 18

$$L^b_{(MR,inertial)} = -\frac{N_b}{2} . M_{bl} . \Delta_e . y_{G_{bl}} . \Omega^2_{MR} . \Gamma . \beta_{1s} \tag{36a}$$

$$M^b_{(MR,inertial)} = -\frac{N_b}{2} . M_{bl} . \Delta_e . y_{G_{bl}} . \Omega^2_{MR} . \beta_{1c} \tag{36b}$$

For the main rotor torque (i.e. yaw moment), we simplify the description by only considering the induced and profile components of a rotor in vertical flight,[17] hence omitting forward flight components

$$N^b_{(MR,aero)} = \Gamma . \Big(-\lambda . C_{TMR} + \sigma_{MR} . CD_{MR}/8 . \Big[1 + 4.6\mu^2_{xy}\Big]\Big) . \rho . \pi . R^3_{rot} . V^2_{MRref} \tag{37}$$

Next, and by adding the main rotor forces times the respective moment arms, we obtain the total main rotor moments as

$$\begin{pmatrix} M_{x_{MR}} \\ M_{y_{MR}} \\ M_{z_{MR}} \end{pmatrix}^{b} = \begin{pmatrix} L_{(MR,flap)} + L_{(MR,inertial)} + y_H . F_{z_{MR}} - z_H . F_{y_{MR}} \\ M_{(MR,flap)} + M_{(MR,inertial)} + z_H . F_{x_{MR}} - x_H . F_{z_{MR}} \\ N_{(MR,aero)} + x_H . F_{y_{MR}} - y_H . F_{x_{MR}} \end{pmatrix}^{b} \tag{38}$$

ROTOR RPM DYNAMICS The main rotor RPM dynamics is related to the available and required power by the following expression[21]

$$N_b.I_b.\Omega_{MR}.\dot{\Omega}_{MR} = P_{shaft} - P_{req} \tag{39}$$

With P_{shaft} the available shaft power, and P_{req} the required power to keep the vehicle aloft. This latter is the sum of main rotor induced and profile power, tail rotor induced and profile power, power plant transmission losses, vehicle parasite power (i.e. drag due to fuselage, landing skids, rotor hub, etc), and finally main rotor, tail rotor, and fuselage aerodynamic interference losses.[27]

Considering the case of an engine failure, a first-order response in P_{shaft} is generally assumed to represent the power decay for turboshaft engines,[28,29] we have

$$\dot{P}_{shaft} = -\frac{P_{shaft}}{\tau_p} \tag{40}$$

With τ_p a to-be-identified time constant. For the required power P_{req}, we simplify the model by only considering the contributions from the main rotor as

$$P_{MR} = \Theta_{MRpwr}.N_{(MR,aero)}.\Omega_{MR} \tag{41}$$

with Θ_{MRpwr} an additional empirical coefficient, which will be addressed in Section III.

II.C. Tail Rotor Modeling

II.C.1. Assumptions

Structural simplifications

- The blade has zero twist, constant chord, zero sweep, and has constant thickness ratio.
- The blade is rigid, hence torsion is neglected.

Aerodynamics simplifications

- Linear lift with constant lift curve slope, and uniform induced flow over the rotor.
- Aerodynamic interference effects from the main rotor is neglected, although this may well be an over-simplification, for some flight conditions.[30,31] Similarly, the aerodynamic interference from the vertical tail (due to blockage) is also neglected.
- Compressibility, blade stall and viscous flow effects are disregarded.

Dynamical simplifications

- No blade dynamics and simplified inflow dynamics.
- Unsteady effects neglected.

II.C.2. Modeling

The tail rotor is a powerful design solution for torque balance, directional stability and control of single main rotor helicopters. The theory we apply here is based on the work done by Bailey in Ref. 32. The model represents a standard approach towards tail rotor modeling, as implemented among others in Ref. 22,33,34.

VELOCITIES The tail rotor hub aerodynamic velocity in the body frame is given by

$$\mathbf{V}^b_{a,TR} = \begin{pmatrix} V_{a,TR_u} \\ V_{a,TR_v} \\ V_{a,TR_w} \end{pmatrix}^b = \begin{pmatrix} u + (q - q_w).z_{TR} - (r - r_w).y_{TR} \\ v - (p - p_w).z_{TR} + (r - r_w).x_{TR} \\ w + (p - p_w).y_{TR} - (q - q_w).x_{TR} \end{pmatrix}^b - \begin{pmatrix} u_w \\ v_w \\ w_w \end{pmatrix}^b \tag{42}$$

In the tail rotor frame F_{TR} of Ref. 33, we have

$$\mathbf{V}^{TR}_{a,TR} = \begin{bmatrix} 1 & 0 & 0 \\ 0 & 0 & 1 \\ 0 & -1 & 0 \end{bmatrix} . \mathbf{V}^b_{a,TR} \tag{43}$$

The non-dimensional velocities in frame F_{TR} are expressed as follows

$$\mu_{TRx} = V^{TR}_{a,MR_u} / V_{TRref} \tag{44a}$$
$$\mu_{TRy} = V^{TR}_{a,MR_v} / V_{TRref} \tag{44b}$$
$$\mu_{TRz} = \Gamma . V^{TR}_{a,MR_w} / V_{TRref} \tag{44c}$$
$$\mu_{TRxy} = \sqrt{\mu^2_{TRx} + \mu^2_{TRy}} \quad \text{and} \quad V_{TRref} = \Omega_{TR} . R_{rot_{TR}} \tag{44d}$$

INFLOW The theory we apply here is based on the work done by Bailey in Ref. 32, implemented among others in Ref. 22, 33, 34. The model given in this paper is a simplified approach of the Bailey model. First, the tail rotor blade pitch is given by

$$\theta_{TR} = \theta_{0_{TR}} - T_{TR} . \frac{\partial \beta_{0_{TR}}}{\partial T_{TR}} . \tan \delta_{3_{TR}} + \theta_{bias_{TR}} \tag{45}$$

The Bailey coefficients are given next by

$$t_1 = \frac{B^2_{TR}}{2} + \frac{\mu^2_{TRxy}}{4} \tag{46a}$$
$$t_2 = \frac{B^3_{TR}}{3} + \frac{B_{TR} . \mu^2_{TRxy}}{2} \tag{46b}$$

Assuming zero twist for the tail rotor blades, the inflow is then derived using momentum theory

$$\lambda_{dw} = \frac{CL_{TR_\alpha} . \sigma_{TR}}{2} . \left(\frac{\mu_{TRz} . t_1 + \theta_{TR} . t_2}{2\sqrt{\mu^2_{TRxy} + \lambda^2_{TR}} + \frac{CL_{TR_\alpha} . \sigma_{TR}}{2} . t_1} \right) \tag{47}$$

And the total tail rotor inflow is given by

$$\lambda_{TR} = \lambda_{dw} - \mu_{TRz} \tag{48}$$

Where it is common practice to iterate between Eq (47) and Eq (48) until convergence within a reasonable tolerance.

FORCES The tail rotor thrust is given by

$$T_{TR} = 2/K_{TR_{corr}}.\lambda_{dw}.\sqrt{\mu_{TRxy}^2 + \lambda_{TR}^2}.\rho.\pi.\left(\Omega_{TR}.R_{rot_{TR}}^2\right)^2 \tag{49}$$

Finally in the body frame we have

$$\begin{pmatrix} F_{x_{TR}} \\ F_{y_{TR}} \\ F_{z_{TR}} \end{pmatrix}^b = \begin{pmatrix} 0 \\ \Gamma.T_{TR} \\ 0 \end{pmatrix} \tag{50}$$

Where we have neglected any aerodynamic interference effects with the main rotor and vertical tail (e.g. blockage effect).

MOMENTS The tail rotor moments are primarily due to the tail rotor force times the respective moment arms. For completeness we also add the rotor torque acting on the pitch axis,[17] we get

$$\begin{pmatrix} M_{x_{TR}} \\ M_{y_{TR}} \\ M_{z_{TR}} \end{pmatrix}^b = \begin{pmatrix} -z_{TR}.T_{TR} \\ \sigma_{TR}.CD_{TR}/8.(1 + 4.6\mu_{TRxy}^2).\rho.\pi.\Omega_{TR}^2.R_{rot_{TR}}^5 \\ x_{TR}.T_{TR} \end{pmatrix} \tag{51}$$

II.D. Fuselage Modeling

The flow around the fuselage is characterized by strong nonlinearities, and is further distorted by the influence of the main rotor wake. Hence, the associated forces and moments, due to the surface pressures and skin friction, are complex functions of flight speed and direction.[15] Indeed, it is well-known that important unsteady separation effects exist, but are rather complex to model.[15]

II.D.1. Assumptions

Aerodynamics Simplifications

- Fuselage aerodynamic center collocated with vehicle CG.
- Effect of rotor downwash on fuselage is neglected. It can however be modeled as in Ref. 35, using a polynomial in wake skew angle, where the polynomial coefficients need to be fit from flight data.[36]
- Only steady airloads effects on the fuselage are considered.

II.D.2. Modeling

The fuselage model is based upon aerodynamic lift and drag coefficients, which are tabulated as a function of airflow angle of attack and sideslip angles. For low speed sideways flight, the important fuselage characteristics are in general, the sideforce, vertical drag, and yawing moment. While in forward flight, the three most important characteristics include drag, and pitching and yawing moments variations with incidence and sideslip.[15] The fuselage rolling moment is usually small, except for configurations with deep hulls where the fuselage aerodynamic center may be significantly below the vehicle CG.[15] For additional information, see also Ref. 37, 38.

VELOCITIES AND AIRFLOW ANGLES The fuselage aerodynamic velocity, at its aerodynamic center, in the body frame is given by

$$\mathbf{V}^b_{a,F} = \begin{pmatrix} V_{a,F_u} \\ V_{a,F_v} \\ V_{a,F_w} \end{pmatrix}^b = \begin{pmatrix} u + (q - q_w).z_F - (r - r_w).y_F \\ v - (p - p_w).z_F + (r - r_w).x_F \\ w + (p - p_w).y_F - (q - q_w).x_F \end{pmatrix}^b - \begin{pmatrix} u_w \\ v_w \\ w_w \end{pmatrix}^b \tag{52}$$

The fuselage angle of attack is given by

$$\alpha_F = \arctan(V_{a,F_w}/|V_{a,F_u}|) \tag{53}$$

And the fuselage sideslip angle is given as in Ref. 13 by

$$\begin{array}{rcl} \beta_F & = & \arcsin(V_{a,F_v}/V_{a,F}) \quad \text{if} \quad V_{a,F_u} \geq 0 \\ \beta_F & = & \pi/2 + \arccos(V_{a,F_v}/V_{a,F}) \quad \text{if} \quad V_{a,F_u} < 0 \quad \text{and} \quad V_{a,F_v} \geq 0 \\ \beta_F & = & -\pi/2 - \arccos(-V_{a,F_v}/V_{a,F}) \quad \text{if} \quad V_{a,F_u} < 0 \quad \text{and} \quad V_{a,F_v} < 0 \end{array} \tag{54}$$

With $V_{a,F} = \sqrt{V^2_{a,F_u} + V^2_{a,F_v} + V^2_{a,F_w}}$.

FORCES In the body frame F_b we have

$$\begin{array}{rcl} F^b_{x_F} & = & q_{dp}.Cx^b_F(\alpha_F, \beta_F) \\ F^b_{y_F} & = & q_{dp}.Cy^b_F(\alpha_F, \beta_F) \\ F^b_{z_F} & = & q_{dp}.Cz^b_F(\alpha_F, \beta_F) \\ q_{dp} & = & 1/2.\rho.S_{ref_F}.V^2_{a,F} \end{array} \tag{55}$$

The aerodynamic coefficients $Cx_F(.)$, $Cy_F(.)$, and $Cz_F(.)$ are tabulated as a function of airflow angle of attack α_F, and sideslip angle β_F. These lookup tables have been derived from a scaled-down full-size helicopter fuselage aerodynamic model.

MOMENTS In the body frame F_b we have

$$\begin{array}{rcl} M^b_{x_F} & = & q_{dp}.Mx_F(\alpha_F, \beta_F).L_{ref_F} \\ M^b_{y_F} & = & q_{dp}.My_F(\alpha_F, \beta_F).L_{ref_F} \\ M^b_{z_F} & = & q_{dp}.Mz_F(\alpha_F, \beta_F).L_{ref_F} \\ q_{dp} & = & 1/2.\rho.S_{ref_F}.V^2_{a,F} \end{array} \tag{56}$$

Here too, the aerodynamic coefficients $Mx_F(.)$, $My_F(.)$, and $Mz_F(.)$ are tabulated as a function of airflow angle of attack α_F, and sideslip angle β_F. These lookup tables have also been derived from a scaled-down full-size helicopter fuselage aerodynamic model.

II.E. Vertical Tail Modeling

The role of the vertical tail is twofold: (i) in forward flight, it generates a sideforce and yawing moment, hence reducing the tail rotor thrust requirement, in order to increase the fatigue life of the tail rotor,[15,21] and (ii) during maneuvers, and during wind gusts, it provides yaw damping and stiffness, enhancing directional stability.[15]

II.E.1. Assumptions

Aerodynamics Simplifications

- Effect of main rotor downwash on vertical tail is neglected. It can however be modeled by using flat vortex wake theory[39] (valid for small sideslip angles), as presented in Ref. 40, 41, or it may be modeled as a polynomial in wake skew angle as in Ref. 35.
- As an aside, the effect of the main rotor downwash on the tail boom is neglected, but ought to be considered at low speed, since it may influence yaw damping.[15]

II.E.2. Modeling

The vertical tail is basically a wing,[19,20] several modeling approaches can be found in Ref. 22, 35, 37, 38. Here, we use a flat plate representation.

VELOCITIES AND AIRFLOW ANGLES The vertical tail aerodynamic velocity, at its aerodynamic center, in the body frame is given by

$$\mathbf{V}^b_{a,VT} = \begin{pmatrix} V_{a,VT_u} \\ V_{a,VT_v} \\ V_{a,VT_w} \end{pmatrix}^b = \begin{pmatrix} u + (q - q_w).z_{VT} - (r - r_w).y_{VT} \\ v - (p - p_w).z_{VT} + (r - r_w).x_{VT} \\ w + (p - p_w).y_{VT} - (q - q_w).x_{VT} \end{pmatrix}^b - \begin{pmatrix} u_w \\ v_w \\ w_w \end{pmatrix}^b \tag{57}$$

Since in the sequel we will neglect the spanwise flow (along the z-axis), we have $V_{a,VT} = \sqrt{V^2_{a,VT_u} + V^2_{a,VT_v}}$.

And the vertical tail angle of attack is given by

$$\begin{array}{rcl} \alpha_{VT} & = & -\arctan(V_{a,VT_v}/V_{a,VT_u}) \quad \text{if} \quad V_{a,VT_u} \geq 0 \\ \alpha_{VT} & = & -\pi/2 + \arctan(V_{a,VT_u}/V_{a,VT_v}) \quad \text{if} \quad V_{a,VT_u} < 0 \quad \text{and} \quad V_{a,VT_v} \geq 0 \\ \alpha_{VT} & = & \pi/2 + \arctan(V_{a,VT_u}/V_{a,VT_v}) \quad \text{if} \quad V_{a,VT_u} < 0 \quad \text{and} \quad V_{a,VT_v} < 0 \end{array} \tag{58}$$

FORCES In the body frame F_b we have

$$\begin{array}{rcl} F^b_{x_{VT}} & = & q_{dp}.Cx_{VT}(CL, CD, \alpha_{VT}) \\ F^b_{y_{VT}} & = & q_{dp}.Cy_{VT}(CL, CD, \alpha_{VT}) \\ F^b_{z_{VT}} & = & 0 \\ q_{dp} & = & 1/2.\rho.S_{ref_{VT}}.V^2_{a,VT} \end{array} \tag{59}$$

The aerodynamic coefficients $Cx_{VT}(.)$ and $Cy_{VT}(.)$ are first functions of the lift $CL(.)$ and drag $CD(.)$ aerodynamic coefficients of a flat plate. Additionally the $Cx_{VT}(.)$ and $Cy_{VT}(.)$ coefficients are also functions of the airflow angle of attack α_{VT}, through the aerodynamic forces projection on the body frame F_b. Further the $CL(.)$ and drag $CD(.)$ coefficients are also tabulated as a function of airflow angle of attack and Mach number.

MOMENTS The vertical tail moments are due to the tail forces times the respective moment arms, and to the aerodynamic pitch moment of a flat plate. This aerodynamic moment produces a yaw moment about the vehicle CG. In the body frame F_b we have

$$\begin{array}{rcl} M^b_{x_{VT}} & = & -z_{VT}.F_{y_{VT}} \\ M^b_{y_{VT}} & = & z_{VT}.F_{x_{VT}} \\ M^b_{z_{VT}} & = & x_{VT}.F_{y_{VT}} - y_{VT}.F_{x_{VT}} + q_{dp}.Mz_{VT}.L_{ref_{VT}} \\ q_{dp} & = & 1/2.\rho.S_{ref_{VT}}.V^2_{a,VT} \end{array} \tag{60}$$

Here the aerodynamic coefficient $Mz_{VT}(.)$ represents the pitch aerodynamic coefficient of a flat plate. This latter coefficient is tabulated as a function of airflow angle of attack and Mach number.

II.F. Horizontal Tail Modeling

The role of the horizontal tail is also twofold: (i) in forward flight, it generates a trim load that reduces the main rotor fore-aft flapping, and (ii) during maneuvers, and during wind gusts, it provides pitch damping and stiffness, enhancing pitch stability.[15]

II.F.1. Assumptions

Aerodynamics Simplifications

- Effect of main rotor downwash on horizontal tail is neglected. Again it can be modeled by using flat vortex wake theory[39] (valid for small sideslip angles), as presented in Ref. 40,41, or it may be modeled as a polynomial in wake skew angle as in Ref. 35.

II.F.2. Modeling

Here too, we use a flat plate representation. Again, more sophisticated models exist,[19,20] and several approaches can be found in Ref. 22,35,37,38. It is also well-known that, depending on the longitudinal and vertical position of the horizontal tail with respect to the main rotor, erratic longitudinal trim shifts may happen when the helicopter is transitioning from hover to forward flight,[21] as the main rotor wake impinges on the tail surface.[15]

Velocities And Airflow Angles The horizontal tail aerodynamic velocity, at its aerodynamic center, in the body frame is given by

$$\mathbf{V}^b_{a,HT} = \begin{pmatrix} V_{a,HT_u} \\ V_{a,HT_v} \\ V_{a,HT_w} \end{pmatrix}^b = \begin{pmatrix} u + (q - q_w).z_{HT} - (r - r_w).y_{HT} \\ v - (p - p_w).z_{HT} + (r - r_w).x_{HT} \\ w + (p - p_w).y_{HT} - (q - q_w).x_{HT} \end{pmatrix}^b - \begin{pmatrix} u_w \\ v_w \\ w_w \end{pmatrix}^b \tag{61}$$

Since in the sequel we will neglect the spanwise flow (along the y-axis), we have $V_{a,HT} = \sqrt{V^2_{a,HT_u} + V^2_{a,HT_w}}$.

And the horizontal tail angle of attack is given by

$$\begin{array}{rcl} \alpha_{HT} & = & \arctan(V_{a,HT_w}/V_{a,HT_u}) \quad \text{if} \quad V_{a,HT_u} \geq 0 \\ \alpha_{HT} & = & \pi/2 + \arctan(-V_{a,HT_u}/V_{a,HT_w}) \quad \text{if} \quad V_{a,HT_u} < 0 \quad \text{and} \quad V_{a,HT_w} \geq 0 \\ \alpha_{HT} & = & -\pi/2 - \arctan(V_{a,HT_u}/V_{a,HT_w}) \quad \text{if} \quad V_{a,HT_u} < 0 \quad \text{and} \quad V_{a,HT_w} < 0 \end{array} \tag{62}$$

Forces In the body frame F_b we have

$$\begin{array}{rcl} F^b_{x_{HT}} & = & q_{dp}.Cx_{HT}(CL, CD, \alpha_{HT}) \\ F^b_{y_{HT}} & = & 0 \\ F^b_{z_{HT}} & = & q_{dp}.Cz_{HT}(CL, CD, \alpha_{HT}) \\ q_{dp} & = & 1/2.\rho.S_{ref_{HT}}.V^2_{a,HT} \end{array} \tag{63}$$

Again, the aerodynamic coefficients $Cx_{HT}(.)$ and $Cz_{HT}(.)$ are first functions of the lift $CL(.)$ and drag $CD(.)$ aerodynamic coefficients of a flat plate. Additionally the $Cx_{HT}(.)$ and $Cz_{HT}(.)$ coefficients are also functions of the airflow angle of attack α_{HT}, through the aerodynamic forces projection on the body frame F_b. Further the $CL(.)$ and drag $CD(.)$ coefficients are also tabulated as a function of airflow angle of attack and Mach number.

MOMENTS The horizontal tail moments are first due to the tail forces times the respective moment arms, and further are also due to the aerodynamic pitch moment of a flat plate. This aerodynamic moment produces a pitch moment about the vehicle CG. In the body frame F_b we have

$$\begin{array}{lcl} M^b_{x_{HT}} & = & y_{HT}.F_{z_{HT}} \\ M^b_{y_{HT}} & = & z_{HT}.F_{x_{HT}} - x_{HT}.F_{z_{HT}} + q_{dp}.My_{HT}.L_{ref_{HT}} \\ M^b_{z_{HT}} & = & -y_{HT}.F_{x_{HT}} \\ q_{dp} & = & 1/2.\rho.S_{ref_{HT}}.V^2_{a,HT} \end{array} \tag{64}$$

Here too the aerodynamic coefficient $My_{HT}(.)$ represents the pitch aerodynamic coefficient of a flat plate. This latter coefficient is tabulated as a function of airflow angle of attack and Mach number.

III. Black-Box Modeling

A BB model may often be viewed as an empirical, yet simple, system representation, and its purpose is generally threefold, namely (i) to compensate for inaccuracies in model parameters (e.g. CG position, vehicle inertia, flap stiffness, flap hinge offset), (ii) to compensate for not sufficiently well understood areas of a WB model (unmodeled high-order dynamics and/or unmodeled nonlinearities), and (iii) to replace computationally intensive WB sub-systems.

Now since attitude angles and inertial position are readily derived from the linear and rotational velocities, see Eq (2) and Eq (5), it is clear that the crucial states in our model are (u, v, w), (p, q, r), and the MR RPM Ω_{MR}. Hence, the goal of the BB model is to enhance the overall helicopter model accuracy, by improving the behavior of these seven states. This BB model is thus based on seven empirical coefficients, see also Appendix A, defined as

- Three force coefficients $(\Theta_{Fx}\ \Theta_{Fy}\ \Theta_{Fz})^T$ to better fit the body linear velocities (u, v, w), see Eq (7).
- Three moment coefficients $(\Theta_{Mx}\ \Theta_{My}\ \Theta_{Mz})^T$ to better fit the body rotational velocities (p, q, r), see Eq (8).
- One MR power coefficient Θ_{MRpwr} to better fit the MR RPM Ω_{MR} dynamics, since we omitted the contributions due to forward flight when deriving an expression for the main rotor torque, see Eq (41).

The presence of these coefficients allows for a versatile enough modeling framework, which permits us to conjecture that the true system is believed to lie inside the representation capacity of our GB modeling structure. We present next the identification method that is used to estimate these empirical coefficients.

III.A. Identification Through Nonlinear Optimal Control

The aim here is to identify the seven empirical coefficients, regrouped in $\boldsymbol{\Theta}(t)$

$$\forall t \geq 0 \qquad \boldsymbol{\Theta}(t) = \Big(\ \Theta_{Fx}(t) \quad \Theta_{Fy}(t) \quad \Theta_{Fz}(t) \quad \Theta_{Mx}(t) \quad \Theta_{My}(t) \quad \Theta_{Mz}(t) \quad \Theta_{MRpwr}(t) \ \Big)^T \tag{65}$$

We use a time-domain identification method, formulated as a continuous-time, nonlinear, constrained, optimal control problem. Note that since flight data is not available at this stage, the FLIGHTLAB nonlinear simulation model is used as a proxy, albeit in a noise-free setting, for experimental data. In the sequel, the given thirteen-state vector originating from FLIGHTLAB is denoted as $\mathbf{x}_{FL}$, and the corresponding four-control input vector as $\mathbf{u}_{FL}$. Note that this thirteen-state vector corresponds to rigid body and RPM parameters (either measured or estimated through extended/unscented Kalman filtering), which are delivered by any standard helicopter UAV avionics unit. We assume also that an observed Input-Ooutput signal sequence $\mathcal{Z}^N := \big\{(\mathbf{u}_{FL}(t_i), \mathbf{x}_{FL}(t_i))\big\}_{i=1}^N$, collected under the desired operating conditions[o], is available for

[o]Basically a set of trajectories spanning the vehicle's flight envelope.

the identification.

We consider the following problem, consisting in minimizing the Bolza cost functional $J(\mathbf{x}(t), \mathbf{\Theta}(t), T_o, T_f)$, with the state-vector $\mathbf{x}(t)$, and control input-vector $\mathbf{\Theta}(t)$, both defined on compact sets $\mathbf{x}(t) \in \mathcal{P}_x \subseteq \mathbb{R}^{n_x}$, $\mathbf{\Theta}(t) \in \mathcal{P}_\Theta \subseteq \mathbb{R}^{n_\Theta}$, denoting the feasible state and control spaces respectively, with $n_x = 13$ and $n_\Theta = 7$ in our case. Further, the independent time variable t is defined over the time domain $\Omega = (T_o, T_f)$, where the final time T_f may be free or fixed. Note that T_o and T_f do not necessarily represent the initial and final time in set $\mathcal{Z}^N$, since it is generally not computationally tractable to estimate $\mathbf{\Theta}(t)$, for a large set $\mathcal{Z}^N$, in one shot. Rather, the time domain Ω may equally refer to a sub-set of the data present in $\mathcal{Z}^N$, implying that the optimization procedure outlined hereunder may need to be repeated for each new Ω, in which case the result of any optimization problem will serve as an initial value for the subsequent one.

We define next the cost functional

$$J(\mathbf{x}(t), \mathbf{\Theta}(t), T_o, T_f) := \Phi(\mathbf{x}(T_o), T_o, \mathbf{x}(T_f), T_f) + \int_\Omega \Psi(\mathbf{x}(t), \mathbf{\Theta}(t), t)dt \tag{66}$$

In the general problem formulation, the cost functional $J(\cdot)$ has contributions from a fixed cost $\Phi(\cdot)$, and a running cost over time $\int_\Omega \Psi(\cdot)dt$. Additionally, this cost functional $J(\cdot)$ is subject to the system dynamic constraints (see Section II), where the usual representation is given by a set of Ordinary Differential Equations (ODEs), of the form

$$\dot{\mathbf{x}} = f(\mathbf{x}(t), \mathbf{\Theta}(t), t) \quad t \in \Omega \tag{67}$$

The initial and final-time boundary inequality conditions are given by

$$\begin{aligned} B_o(\mathbf{x}(T_o), \mathbf{\Theta}(T_o), T_o) &\leq 0 \\ B_f(\mathbf{x}(T_f), \mathbf{\Theta}(T_f), T_f) &\leq 0 \end{aligned} \tag{68}$$

which may describe the initial and final trimmed flight conditions. Conjointly any algebraic trajectory inequality constraints are given by

$$T(\mathbf{x}(t), \mathbf{\Theta}(t), t) \leq 0 \quad t \in \Omega \tag{69}$$

having a fourfold objective: (i) account for vehicle's inherent physical and flight envelope limitations (bounds on speeds, attitude, and main rotor RPM), (ii) account for environmental constraints (the helicopter cannot descend below ground), (iii) prescribe the actuator control inputs $\mathbf{u}(t) = \mathbf{u}_{FL}(t)$, and (iv) bound any modeling misfits by $||\mathbf{x}(t) - \mathbf{x}_{FL}(t)||_2 \leq \epsilon$, with ϵ small. For generality, the boundary and trajectory constraints Eq (68)-Eq (69) have been expressed as inequality constraints, equality constraints can simply be enforced by equating upper and lower bounds. Further, in Eq (66)-Eq (69) the functions $\Phi(\cdot)$, $\Psi(\cdot)$, $f(\cdot)$, $B_o(\cdot)$, $B_f(\cdot)$, and $T(\cdot)$ are assumed to be sufficiently smooth, i.e. at least C^2. Finally, the solution to the trajectory planning gives the optimal empirical coefficients, which minimize the cost functional $J(\cdot)$, while enforcing the here-above predefined constraints

$$\hat{\mathbf{\Theta}}(t) := \arg \min_{\mathbf{\Theta}(t) \in \mathcal{P}_\Theta} J(\mathbf{x}(t), \mathbf{\Theta}(t), T_o, T_f) \tag{70}$$

III.B. Direct Optimal Control and The Pseudospectral Discretization

We chose to solve our problem through a direct optimal control method. In this context, the continuous-time optimal control problem is first discretized in some manner and the problem is transcribed to a NonLinear Programming problem (NLP),[42–44] without formulating an alternate set of optimality conditions as done through indirect methods.[45–48] The resulting NLP can be solved numerically, by well known and efficient optimization techniques, such as Sequential Quadratic Programming (SQP) methods[49–51] or Interior Point (IP) methods.[52–56] These methods in turn attempt to satisfy a set of conditions called the Karush-Kuhn-Tucker (KKT) conditions.[42] Now regarding the discretization of the continuous-time optimal control problem, the three most common discretization approaches to solve an indirect or direct method are: (i) Single-Shooting (SS),[57] (ii) Multiple-Shooting (MS),[58,59] and (iii) State and Control Parameterization (SCP) methods;[60–64] this latter is sometimes also known as transcription in the aerospace community, or as simultaneous strategy

in the chemical and process community. Here SS and MS approaches are so-called control parameterization techniques where the control signals alone are discretized,[65] whereas in SCP as indicated by its name, both state and control are parameterized.[66]

Briefly summarized, in shooting techniques the dynamics are satisfied by integrating the differential equations using a time-marching algorithm. The advantage of direct SS is that it generates a small number of variables, while its main disadvantage is that a small change in the initial condition can produce a very large change in the final conditions.[67] Further, the issue of stability is a major concern. Indeed, time integration over a relatively large shooting segment may lead to catastrophic results for unstable systems, and this is why SS generally fails to get a converged solution for such systems.[68] The SS has been most successful in launch vehicle trajectories and orbit transfer problems, primarily because this class of problem lends itself to parameterization with a relatively small number of variables.[69]

On the other hand, direct MS breaks the problem into shorter steps,[67] greatly enhancing the robustness of the shooting method, at the cost of having a larger number of variables. It is then primordial to exploit matrix sparsity to efficiently solve the NLP equations.[69] Despite the increased size of the problem, the direct MS method is an improvement over the standard direct SS method because the sensitivity to errors in the unknown initial conditions is reduced, since the differential equations are integrated over significantly smaller time intervals. Further, MS have shown to be suited for applications of high complexity, having large number of states.[70] However, an additional difficulty exists with the shooting techniques, namely the necessity of defining constrained and unconstrained subarcs a priori, when solving problems with path inequality constraints.[69] This issue however does not exist with SCP methods,[71] which is one of the reasons why SCP methods have actively being investigated.[69]

In addition, SCP methods are known to be very effective and robust,[70] and SCP techniques have been applied to solve nonlinear optimal control problems, such as in space and launch/reentry applications,[61,62,72–76] in aircraft applications,[61,77–80] in helicopter applications,[81–83] in UAV applications,[84–86] and glider applications.[87] Since SCP methods have been intensively researched in the last decade, we present next a general overview of this concept. In SCP, several discretization procedures have been studied, namely local Runge-Kutta methods in Ref. 65, 66, 88, 89, local orthogonal methods in Ref. 60, 62, 75, 90, 91, Global Orthogonal Approaches (GOA) or spectral methods in Ref. 91–98, and most recently hybrid local/global methods in Ref. 99. Of these four procedures, the GOA have received much attention in the last decade, since they have the advantage of providing spectral convergence, i.e. at an exponential rate, for the approximation of analytic, i.e. sufficiently smooth, functions.[100–102] Thus, for a given error bound, GOA methods generate a significantly smaller scale optimization problem when compared to other methods.[101] This is an important aspect since the efficiency and even convergence of NLPs improves for a problem of smaller size.[103]

In a GOA the system's state-vector is expressed as a truncated series expansion, characterized by BAsis (BA) functions, and Expansion Coefficients (EC) determined from test functions, which attempt to ensure that the Ordinary Differential Equations (ODEs), defining the system dynamics, are optimally satisfied. The choice of the BA functions is what distinguishes GOA methods from finite-difference or finite-element methods. In both finite-type methods, the BA is local in character, while for GOA methods the BA consists of infinitely differentiable global functions, such as orthogonal polynomials,[104] trigonometric functions, or constant basis function like Haar[105] or block-pulse. Further, the EC distinguish the three most common types of GOA methods, namely Galerkin, Tau, and collocation. Of these three, the last one, often referred to as the PseudoSpectral (PS) discretization, has received considerable attention in recent years. In PS methods, the BA is described by Lagrange interpolating polynomials,[106] and are expressed using a set of N support points. The location of these support points is determined by orthogonal polynomials, for example Legendre polynomials,[104] although other choices exist, such as Chebyshev polynomials.[107] Besides the choice of these N support points, another set of K points is required for the discretization of the integral within the cost functional, and the system dynamic constraints. These K points are chosen such that the quadrature approximation of an integral is minimized.[106] Now, it is well known that the highest accuracy quadrature approximation, for a given number of K points, is the Gauss quadrature.[106] In this case, the location of these K quadrature points, called Legendre-Gauss (LG) points, is determined by the roots of a Kth-degree Legendre polynomial.[94,96] It is also worth noting that two additional variations to the LG approach have

extensively been investigated in the last decade, namely the Legendre-Gauss-Lobatto (LGL) method,[92,93] and the Legendre-Gauss-Radau (LGR) method.[91,97,98] It was further reported in Ref. 108 that the LG and LGR methods have been found to be very similar in accuracy, while outperforming the LGL method.

PS methods have been extensively used in solving fluid dynamics problems,[109,110] but only recently have these methods been used for solving a variety of optimal control problems. It is clear that PS methods exhibit a number of advantages when compared to other discretization methods, even when compared to the popular spline parametrization.[67,84,111] Indeed, PS techniques have been widely used in space and launch/reentry applications, see the results of Ref. 112–129. However, they have so far only seen limited use in other aeronautical applications such as: aircrafts,[117,130–133] helicopters,[134] fixed-wing UAVs,[119,135–138] and helicopter UAVs.[139,140] Accordingly, we opt for a PS numerical structure, as the discretization framework for our identification problem.

Once the optimal empirical values $\hat{\mathbf{\Theta}}(t)$ have been obtained, the following step consists in finding a smooth and continuous-time nonlinear mapping, $g_\Theta(\cdot)$ s.t.

$$\hat{\mathbf{\Theta}}(t) = g_\Theta(\tilde{\mathbf{x}}(t), \tilde{\mathbf{u}}(t)) \tag{71}$$

with $\tilde{\mathbf{x}} \in \mathbb{R}^{\tilde{n}_x}$, $\tilde{\mathbf{u}} \in \mathbb{R}^{\tilde{n}_u}$, $\tilde{n}_x \leq n_x, \tilde{n}_u \leq n_u$ representing either, the full state and control vectors respectively as given in Eq (1), or a subset of these vectors.

III.C. Neural Networks Model

For physically-intuitive plants, one may select the required states $\tilde{\mathbf{x}}$ and inputs $\tilde{\mathbf{u}}$, based upon engineering judgment, and derive thes nonlinear mapping $g_\Theta(\cdot)$ through popular curve-fitting methods. For non-transparent systems, exhibiting significant dependences among variables, one may consider formal/systematic approaches such as principal component analysis, statistical analysis, fuzzy tools, or Neural Networks (NNs). Now, NNs have found a wide range of applications in control theory. Indeed, under mild assumptions on continuity and boundedness, a network of two layers, the first being hidden sigmoid and the second linear, can be trained to approximate any Input-Output (IO) relationship arbitrarily well, provided the number of neurons L in the hidden layer is high enough.[141,142] Hence, we propose here to anchor the $g_\Theta(\cdot)$ modeling within the NN paradigm.

$$\begin{aligned} \hat{\mathbf{\Theta}}(t) &= g_\Theta(\tilde{\mathbf{x}}(t), \tilde{\mathbf{u}}(t)) = C_\Theta.\mathbf{s}_\Theta(t) \\ \mathbf{s}_\Theta(t) &= W_{o_\Theta}.\kappa\big(W_{x_\Theta}\tilde{\mathbf{x}}(t) + W_{u_\Theta}\tilde{\mathbf{u}}(t) + W_{b_\Theta}\big) \end{aligned} \tag{72}$$

where $W_{o_\Theta} \in \mathbb{R}^{n_\Theta \times L}$ and $W_{x_\Theta} \in \mathbb{R}^{L \times \tilde{n}_x}$, $W_{u_\Theta} \in \mathbb{R}^{L \times \tilde{n}_u}$, contain the output and hidden layer weights respectively. Further, $W_{b_\Theta} \in \mathbb{R}^L$ contains the sets of biases in the hidden layer, $C_\Theta \in \mathbb{R}^{n_\Theta \times n_\Theta}$ contains the output linear map, and $\kappa(\cdot)$ is the activation function, taken as a continuous, diagonal, differentiable, and bounded static sigmoid nonlinearity.

IV. Simulation Results

We implemented our model in a MATLAB® environment.[143] The modeled UAV is an instrumented R/C *Align T-REX* helicopter, belonging to the flybarless two-bladed main rotor class, which physical characteristics as documented in Appendix B. Additionally, for the FLIGHTLAB model, the following options have been selected

- Articulated rotor, and blade element model. Quasi-steady airloads, based on the Peters-He three-state inflow model, with no stall delay effects.
- Bailey tail rotor, and ideal engine.

In this paper, and purely for the sake of illustration, we base the identification on a single trajectory, starting from hover. The applied input corresponds to an 5 s long collective sine-sweep, from 0.1 to 2 Hz,

with an amplitude of 0.5 °. Now, the very low vehicle roll inertia, and the low pitch inertia (see Appendix B) have resulted in very noisy roll and pitch rates, due to blade flapping. Indeed, a power spectral density analysis revealed the presence of a high energy component at the 2/Rev = 45 Hz harmonic. Hence, we decided to low-pass the roll and pitch rates, before using them in the identification, with a zero-phase shift, fifth order, digital Butterworth filter, having a cutoff frequency set at 10 Hz.

To solve the nonlinear control problem of Section III.A, the pseudospectral numerical method, as described in Section III.B, is used. This numerical discretization framework is available in a MATLAB environment, through the open-source General Pseudospectral OPtimal control Software GPOPS®.[95,144–146] In order to use GPOPS, the optimal control problem must first be reformulated into a GPOPS format, as a set of MATLAB m-files.[146] Second, the helicopter model must also be expressed in a vectorized structure, implying that each model variable and parameter is a vector, which values are time-dependent. This latter aspect is particularly relevant for complex models, where for instance standard matrix-matrix multiplications have to be handled with care, as each matrix element is a vector. Third, (cubic) B-Splines interpolating functions ought to be used, when querying lookup tables, as the spectral convergence of PS methods only holds when the functions under consideration are smooth.[104,147] It is also best practice to non-dimensionalize and scale model variables and quantities, in order to improve conditioning of the numerical problem. With respect to the cost functional of Eq (66), we chose to minimize the variance of $\mathbf{\Theta}(t)$, on each $\Omega = (T_o, T_f)$ interval. Next the trajectory constraint $||\mathbf{x}(t) - \mathbf{x}_{FL}(t)||_2 \leq \epsilon$ in Eq (69) has been set to $\epsilon = 10\%$. Further, finite differencing has been used to estimate the objective gradient and constraint Jacobian. Once the control problem discretized, it is then transcribed into a static, finite-dimensional NLP optimization problem. An NLP is generally sparse, and many well-known efficient optimization techniques exist to numerically solve large-scale and sparse NLPs. In our case, we use the SNOPT® software,[51] which solves finite-dimensional optimization problems through SQP.

From a computational tractability and solvability viewpoint, it is preferable to solve a large number of *small* optimization problems - defined each on a very short $\Omega = (T_o, T_f)$ interval and having each very few nodes - than to solve a single *large* optimization problem, defined on a large $\Omega = (T_o, T_f)$ interval with many nodes. Accordingly, we have decided to base the discretization of the optimal problem on just 3 nodes, yielding a NLP problem with 55 variables and 44 constraints. Now since the data provided by FLIGHTLAB is sampled at 540 Hz, we will use a very small $\Omega = (T_o, T_f)$ interval of 9.26 ms, corresponding to a sampling frequency of 540/5=108 Hz. Once the optimal empirical coefficients $\hat{\mathbf{\Theta}}$ have been computed, and before fitting the NN model of Eq (72), we low-pass these coefficients with again a zero-phase shift, fifth order, digital Butterworth filter, having a cutoff frequency set at 2 Hz, in order to remove the unrealistic high-frequency behavior, and any additional outliers. Finally, the NN model of Section III.C is based upon a 5-neurons feedforward network, with a hyperbolic tangent activation transfer function in the hidden layer, and backpropagation training for the weights and biases.

Next, we apply a collective sweep input, at a constant main rotor RPM, to both our estimated model and FLIGHTLAB, and briefly compare the open-loop responses. The simulation plots are given in Appendix C. Figure 1 shows the evolution of the body states, whereas Figure 2 displays the inertial positions and velocities. Compared to the FLIGHTLAB benchmark model, we see that the model's preliminary results are encouraging. Note however that the NN model is rather approximate, since trained with only a single trajectory. Hence, future work shall concentrate on NN modeling improvement, since this latter accounts for most of the misfit between our model and FLIGHTLAB.

V. Conclusion

We have presented a novel methodology, which allows for the formulation of a highly-accurate, yet computationally tractable, grey-box nonlinear helicopter model. The adopted strategy consists in replacing all modeling uncertainty - parameter uncertainties, unmodeled higher-order dynamics, and unmodeled static nonlinearities - by empirical coefficients. Next, the identification of these coefficients has been based upon the combined paradigms of nonlinear optimal control, and Neural Networks (NN). Our preliminary encouraging results invite further application and investigations of the here-presented approach.

Appendix A: Nomenclature

- Frames
  - F_I Geocentric inertial frame
  - F_E Normal earth fixed frame
  - F_o Vehicle carried normal earth frame
  - F_b Body (vehicle) frame
  - F_a Aerodynamic (air path) frame
  - F_k Kinematic (flight path) frame
  - F_{HB} Hub-Body frame
  - F_{HB} Hub-Body frame
  - F_{HBw} Hub-Body wind-axis frame
  - F_{TR} Tail-Rotor frame
- Frame origins
  - A Origin of frame F_I, earth center
  - O Origin of frames F_E and F_o, an earth surface point
  - G Origin of frames F_b, F_a and F_k, aircraft center of mass
- Angles between frames
  - ψ Azimuth angle (yaw angle, heading)
  - θ Inclination angle (pitch angle, or elevation)
  - ϕ Bank angle (roll angle)
- Position
  - x_N, x_E, x_Z Coordinates of CG position vector in F_E frame
  - x_H, y_H, z_H Coordinates of Hub position wrt vehicle CG in F_b frame
- Altitude
  - $h_H = -x_Z - z_H$ Hub position above ground
- Linear velocities are denoted $\mathbf{V}$ and their components u, v, w
  - $\mathbf{V}_{k,G}$ Kinematic velocity of the vehicle center of mass
  - $\mathbf{V}_{a,G}$ Aerodynamic velocity of the vehicle center of mass
  - $u_k^o = V_N$ x component of $\mathbf{V}_{k,G}$ on F_o, V_N North velocity
  - $v_k^o = V_E$ y component of $\mathbf{V}_{k,G}$ on F_o, V_E East velocity
  - $w_k^o = V_Z$ z component of $\mathbf{V}_{k,G}$ on F_o, V_Z Vertical velocity
  - $u_k^b = u$ x component of $\mathbf{V}_{k,G}$ on body frame F_b
  - $v_k^b = v$ y component of $\mathbf{V}_{k,G}$ on body frame F_b
  - $w_k^b = w$ z component of $\mathbf{V}_{k,G}$ on body frame F_b
- Angular velocities are denoted $\mathbf{\Omega}$ and their components p, q, r
  - $\mathbf{\Omega}_k = \mathbf{\Omega}_{bE}$ Kinematic angular velocity of the vehicle (b) relative to the earth (E)
  - $p_k^b = p$ Roll velocity (roll rate) of the vehicle relative to the earth (frame F_E)
  - $q_k^b = q$ Pitch velocity (pitch rate) of the vehicle relative to the earth
  - $r_k^b = r$ Yaw velocity (yaw rate) of the vehicle relative to the earth

- Wind

$\mathbf{V}_w$	Wind linear velocity in F_E, of an atmospheric particle which could have been located at the vehicle center of mass
u_w	Wind x-velocity in F_E
v_w	Wind y-velocity in F_E
w_w	Wind z-velocity in F_E
p_w	Wind roll-velocity in F_E
q_w	Wind pitch-velocity in F_E
r_w	Wind yaw-velocity in F_E
Ψ_w	Wind azimuthal angular position
ρ	Air density

- Mass and Inertia

m_{Fus} Fuselage mass

$$\mathbb{I}_{Fus} = \begin{bmatrix} A & -F & -E \\ -F & B & -D \\ -E & -D & C \end{bmatrix}$$ Fuselage inertia

- Main Rotor (MR) properties

Γ	Direction of rotation, $CCW : \Gamma = 1 \quad CW : \Gamma = -1$
N_b	Number of blades
M_{bl}	Blade 0th mass moment (blade mass from flap hinge)
$C_0 = M_{bl}.y_{G_{bl}}$	Blade 1st mass moment
I_β	Blade 2nd mass moment (inertia about flap hinge)
I_b	Blade 2nd mass moment (inertia about rotor shaft)
R_{rot}	Rotor radius measured from hub center
R_{bl}	Blade radius measured from flap hinge
Δ_e	Distance between hub and flap hinge
c_{bl}	Blade chord
$y_{G_{bl}}$	Blade CG radial position from flap hinge
$\sigma_{MR} = \frac{N_b.c_{bl}}{\pi.R_{rot}}$	Solidity
B	Tip loss factor, expressed as percentage of blade length R_{bl} no lift is generated outboard of position $B.R_{bl}$
$\gamma = \frac{\rho.c_{bl}.CL_{MR_\alpha}.R_{bl}^4}{I_\beta}$	Blade Lock number
λ_m	Momentum theory induced flow due to rotor thrust (TPP)
λ_h	Rotor induced inflow in hover $\lambda_h = \sqrt{\frac{C_{T_{MR}}}{2}} = v_h/V_{MRref}$
μ	Advance ratio
μ_x	Non-dimensional forward flight air velocity
μ_y	Non-dimensional sidewards flight air velocity
$\mu_{xy} = \sqrt{\mu_x^2 + \mu_y^2}$	Non-dimensional in-plane (rotor disk) air velocity
μ_z	Non-dimensional vertical flight air velocity (normal to the TPP)
K_{S_β}	Hub spring restraint coefficient (due to flap)
$\bar{\mu} = \frac{\mu}{\lambda_h}$	Normalizing advance ratio
$\bar{\lambda} = \frac{\lambda_m + \mu_z}{\lambda_h}$	Normalizing total inflow
G_{eff}	Ground effect corrective factor
$\epsilon = \frac{\Delta_e}{R_{rot}}$	Normalized flap hinge offset

- Main Rotor (MR) properties (Cont'd)
  Θ_{MRpwr} Form factor on rotor power
- MR position vector components
  x_H, y_H, z_H Position of Hub center wrt vehicle CG G
- MR angles
  ψ_{bl} Azimuthal angular position of blade
  β_0 Rotor TPP coning angle
  β_{1c} Longitudinal rotor TPP tilt (positive forward)
  β_{1s} Lateral rotor TPP tilt (positive towards retreating side)
  θ_{bl} Blade pitch outboard of flap hinge (feathering) angle
  ψ_{PA} Swashplate phase angle
  θ_0 Blade root collective pitch
  θ_{1c} Lateral cyclic pitch
  θ_{1s} Longitudinal cyclic pitch
  β_{MR} Sideslip angle

$$\begin{aligned} \beta_{bl} &\simeq \beta_0 + \beta_{1c}\cos\psi_{bl} + \beta_{1s}\sin\psi_{bl} \\ \theta_{bl} &= \theta_0 + \theta_{1c}\cos(\psi_{bl}+\psi_{PA}) + \theta_{1s}\sin(\psi_{bl}+\psi_{PA}) \end{aligned}$$

- MR angular velocities
  $\Omega_{MR_{100\%}}$ Nominal (100%) angular velocity
  Ω_{MR} Instantaneous angular velocity
- MR linear velocities
  v_{i_o} Rotor uniform induced velocity, normal to the TPP and positive when oriented downwards
  v_h Rotor induced velocity in hover
  $v_h = \sqrt{\frac{m.g}{2.\rho.\pi.R_{rot}^2}}$
  V_{MRref} Reference velocity
  $V_{MRref} = \Omega_{MR}.R_{rot}$
- MR forces/moments
  $F_{x_{MR}}$ x-force
  $F_{y_{MR}}$ y-force
  $F_{z_{MR}}$ z-force
  $M_{x_{MR}}$ Total roll moment
  $M_{y_{MR}}$ Total pitch moment
  $M_{z_{MR}}$ Total yaw moment
  $L_{(MR,inertial)}$ Roll moment due to inertia loads
  $M_{(MR,inertial)}$ Pitch moment due to inertia loads
  $L_{(MR,flap)}$ Roll moment due to hub spring restraint (flap)
  $M_{(MR,flap)}$ Pitch moment due to hub spring restraint (flap)
  $N_{(MR,aero)} = Q_{MR}$ Yaw moment due to aerodynamic loads
  P_{MR} Power

- MR aerodynamic and force/moments coefficients
  - C_{HMR} Drag coefficient
  - C_{YMR} Side-force coefficient
  - C_{TMR} Thrust coefficient
  - CL_{MR_α} Blade section lift curve slope
  - CL_{MR} Lift coefficient
  - CD_{MR} Mean drag coefficient (profile drag)
- Tail Rotor (TR) properties
  - $N_{b_{TR}}$ Number of blades
  - $R_{rot_{TR}}$ Rotor radius measured from shaft
  - $\frac{\partial \beta_{0_{TR}}}{\partial T_{TR}}$ Partial coning angle wrt thrust
  - $\tan \delta_{3_{TR}}$ Tangent of hinge skew angle for pitch-flap coupling
  - c_{TR} Blade chord
  - $\sigma_{TR} = \frac{N_{b_{TR}}.c_{TR}}{\pi.R_{rot_{TR}}}$ Solidity
  - μ_{TRx} x-component of advance ratio
  - μ_{TRy} y-component of advance ratio
  - $\mu^2_{TRxy} = \mu^2_{TRx} + \mu^2_{TRy}$
  - μ_{TRz} z-component of advance ratio
  - λ_{TR} Total inflow
  - λ_{dw} Inflow
  - $t_1 \quad t_2$ Bailey coefficients
  - CL_{TR_α} Blade section lift curve slope
  - CD_{TR} Mean drag coefficient (profile drag)
  - B_{TR} Tip loss factor, expressed as percentage of blade length
  - $K_{TR_{corr}}$ Correction factor
- TR position vector components
  - x_{TR}, y_{TR}, z_{TR} Position wrt vehicle CG (in F_{HB} frame)
- TR angles
  - $\beta_{0_{TR}}$ Coning angle
  - θ_{TR} Blade pitch angle
  - $\theta_{0_{TR}}$ Blade root collective pitch
  - $\theta_{bias_{TR}}$ Preset collective pitch bias
- TR angular velocities
  - $\Omega_{TR_{100\%}}$ Nominal (100%) angular velocity
  - Ω_{TR} Instantaneous angular velocity
- TR linear velocities
  - $\mathbf{V}_{a,TR}$ Aerodynamic velocity of the TR hub
  - V_{TRref} Reference velocity
    $V_{TRref} = \Omega_{TR}.R_{rot_{TR}}$

- TR forces/moments
  - T_{TR} Thrust
  - $F_{x_{TR}}$ x-force
  - $F_{y_{TR}}$ y-force
  - $F_{z_{TR}}$ z-force
  - $M_{x_{TR}}$ Total roll moment
  - $M_{y_{TR}}$ Total pitch moment
  - $M_{z_{TR}}$ Total yaw moment
- Fuselage (Fus) properties
  - S_{ref_F} Reference area
  - L_{ref_F} Reference length
- Fuselage angles
  - α_F Angle of attack
  - β_F Sideslip angle
- Fuselage position vector components
  - x_F, y_F, z_F Position of fuselage CG wrt
- Fuselage forces/moments
  - F_{x_F} x-force
  - F_{y_F} y-force
  - F_{z_F} z-force
  - M_{x_F} Total roll moment
  - M_{y_F} Total pitch moment
  - M_{z_F} Total yaw moment
- Horizontal/Vertical Tails (HTVT) properties
  - $S_{ref_{HT}}$ HT Reference area
  - $L_{ref_{HT}}$ HT Reference length
  - $S_{ref_{VT}}$ VT Reference area
  - $L_{ref_{VT}}$ VT Reference length
- Horizontal/Vertical Tails (HTVT) angles
  - α_{HT} HT angle of attack
  - β_{HT} HT sideslip angle
  - α_{VT} VT angle of attack
  - β_{VT} VT sideslip angle
- Horizontal/Vertical Tails (HTVT) position vector components
  - x_{HT}, y_{HT}, z_{HT} Position of horizontal tail aerodynamic center
  - x_{VT}, y_{VT}, z_{VT} Position of vertical tail aerodynamic center

- Horizontal/Vertical Tails (HTVT) forces/moments
  - $F_{x_{HT}}$ HT x-force
  - $F_{y_{HT}}$ HT y-force
  - $F_{z_{HT}}$ HT z-force
  - $F_{x_{VT}}$ VT x-force
  - $F_{y_{VT}}$ VT y-force
  - $F_{z_{VT}}$ VT z-force
  - $M_{x_{HT}}$ Total HT roll moment
  - $M_{y_{HT}}$ Total HT pitch moment
  - $M_{z_{HT}}$ Total HT yaw moment
  - $M_{x_{VT}}$ Total VT roll moment
  - $M_{y_{VT}}$ Total VT pitch moment
  - $M_{z_{VT}}$ Total VT yaw moment
- Empirical coefficients (black-box model)
  - Θ_{Fx} Added on total x-force
  - Θ_{Fy} Added on total y-force
  - Θ_{Fz} Added on total z-force
  - Θ_{Mx} Added on total x-moment
  - Θ_{My} Added on total y-moment
  - Θ_{Mz} Added on total z-moment
  - Θ_{MRpwr} Form factor on MR power

Appendix B: Align T-REX Physical Parameters

	Name	Parameter	Value	Unit
Environment	Air density	ρ	1.2367	kg/m^3
	Static temperature	T	273.15 + 15	K
	Specific heat ratio (air)	γ	1.4	
	Gas constant (air)	R	287.05	$J/kg.K$
	Gravity constant	g	9.812	m/s^2
Vehicle	Total mass	m	7.75	kg
	Inertia moment wrt x_b	A	0.0705	$kg.m^2$
	Inertia moment wrt y_b	B	0.4760	$kg.m^2$
	Inertia moment wrt z_b	C	0.2855	$kg.m^2$
	Inertia product wrt x_b	D	0	$kg.m^2$
	Inertia product wrt y_b	E	0.0018	$kg.m^2$
	Inertia product wrt z_b	F	0	$kg.m^2$
Main Rotor	Direction of rotation	Γ	CW (-1)	
	Number of blades	N_b	2	
	Nominal angular velocity	$\Omega_{MR_{100\%}}$	131.37	rad/s
	Rotor radius from hub	R_{rot}	0.9	m
	Blade mass	M_{bl}	0.208	kg
	Spring restraint coef. due to flap	K_{S_β}	163.8	$N.m/rad$
	Distance between hub and flap hinge	Δ_e	0.32	m
Tail Rotor	Number of blades	2		
	Nominal angular velocity	$\Omega_{TR_{100\%}}$	612.61	rad/s
	Rotor radius from rotor hub	$R_{rot_{TR}}$	0.14	m
Actuators	MR collective	θ_0	[-3,10].π/180	rad
	TR collective	θ_{TR}	[-12,18].π/180	rad
	MR lateral cyclic	θ_{1c}	[-7,7].π/180	rad
	MR longitudinal cyclic	θ_{1s}	[-7,7].π/180	rad
	MR collective rate	$\dot{\theta}_0$	[-52,52].π/180	rad/s
	TR collective rate	$\dot{\theta}_{TR}$	[-120,120].π/180	rad/s
	MR lateral cyclic rate	$\dot{\theta}_{1c}$	[-56,56].π/180	rad/s
	MR longitudinal cyclic rate	$\dot{\theta}_{1s}$	[-56,56].π/180	rad/s

Appendix C: Simulation Results

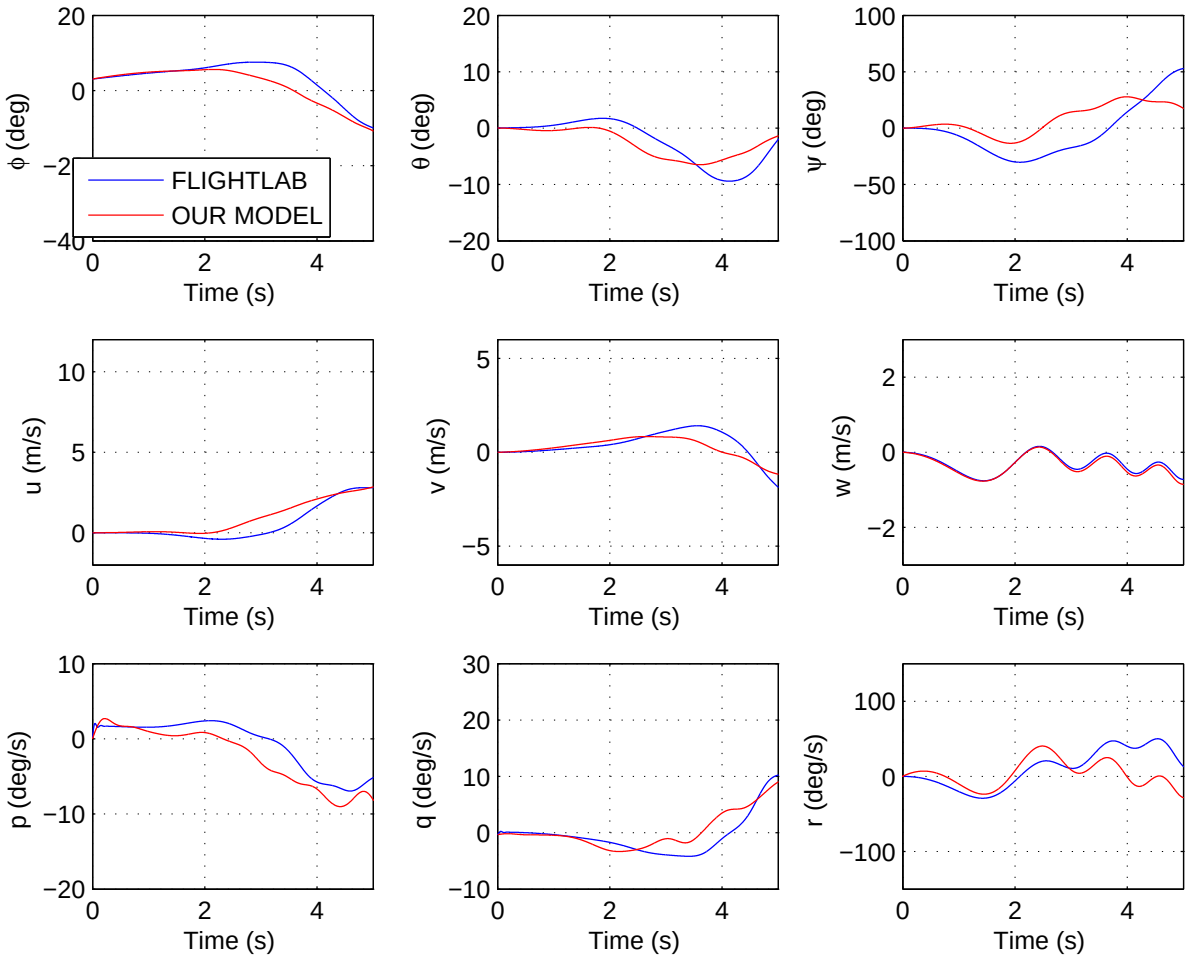

Figure 1. Vehicle response in body frame

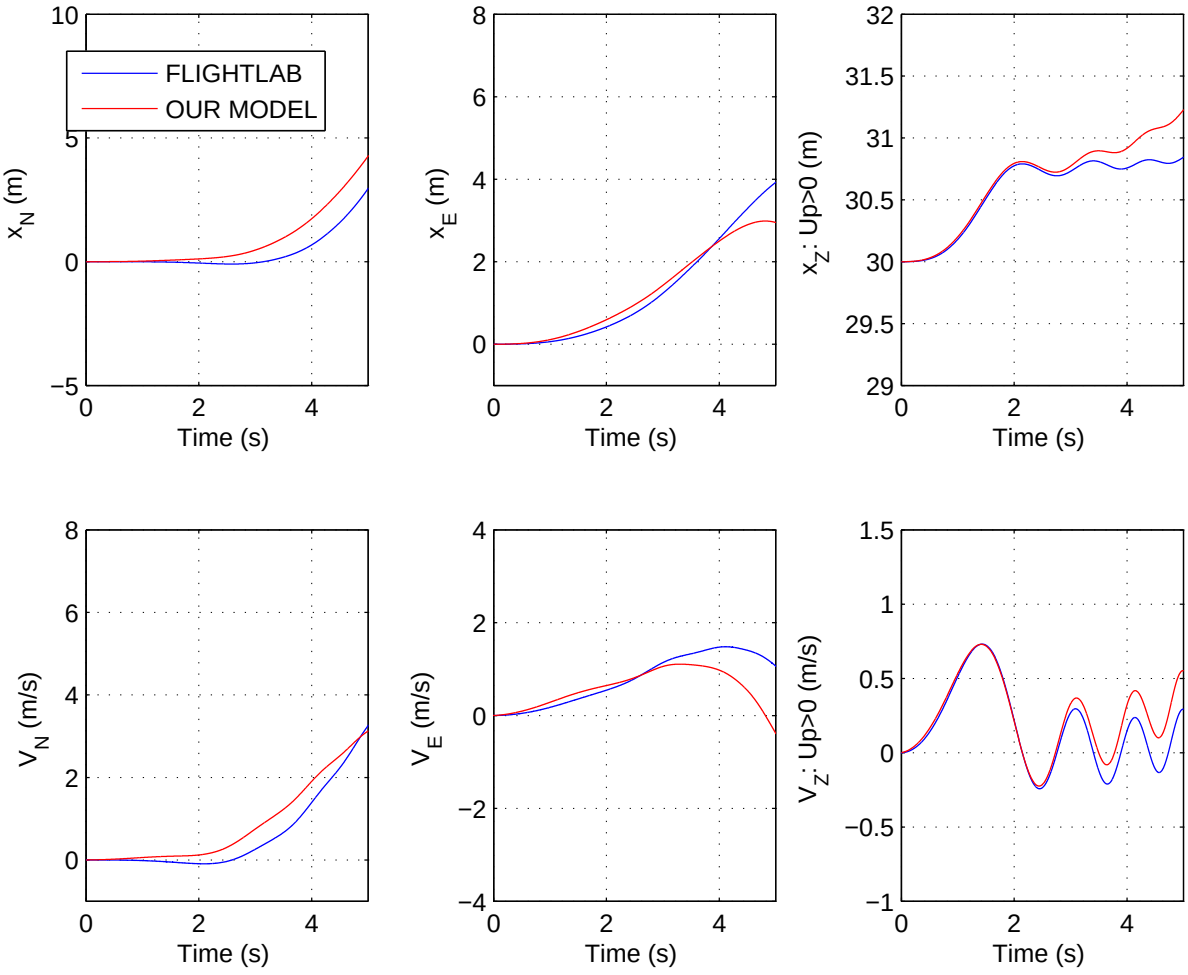

Figure 2. Vehicle response in inertial frame

References

[1]DoD, "Unmanned Aircraft Systems (UAS) Roadmap 2005-2030," Tech. rep., U.S.A. DoD, 2005.

[2]Willems, J. C., "Dissipative Dynamical Systems, Part I: General Theory," *Archive for Rational Mechanics and Analysis*, Vol. 45, 1972, pp. 321–351.

[3]Johansen, T. A., *Operating Regime Based Process Modeling and Identification*, Ph.D. thesis, Norwegian Institute of Technology, 1994.

[4]Angelis, G. Z., *System Analysis, Modelling and Control with Polytopic Linear Models*, Ph.D. thesis, Eindhoven University of Technology, 2001.

[5]Chalmers, A. F., *What is this Thing Called Science ?*, Open University Press, 1982.

[6]Romijn, R., Ozkan, L., Weiland, S., Ludlage, J., and Marquardt, W., "A Grey-Box Modeling Approach For The Reduction Of Nonlinear Systems," *8th Int. IFAC Symposium on Dynamics and Control of Process Systems*, 2007.

[7]Taamallah, S., "Optimal Autorotation With Obstacle Avoidance For A Small-Scale Flybarless Helicopter UAV," *AIAA Guidance, Navigation and Control Conf.*, 2012.

[8]Taamallah, S., Bombois, X., and Van den Hof, P. M. J., "Optimal Control For Power-Off Landing Of A Small-Scale Helicopter A Pseudospectral Approach," *Am. Control Conf.*, 2012.

[9]Taamallah, S., "Low-Order Modeling For A Small-Scale Flybarless Helicopter UAV, A Grey-Box Time-Domain Approach," *AIAA Atmospheric Flight Mechanics Conf.*, 2012.

[10]Seckel, E. and Curtiss, H. C., "Aerodynamic Characteristics of Helicopter Rotors," Tech. Rep. No. 659, Department of Aerospace and Mechanical Engineering, Princeton University, 1962.

[11]Chen, R. T. N., "A Simplified Rotor System Mathematical Model for Piloted Flight Dynamics Simulation," Tech. Rep. NTM 78575, NASA Ames Research Center, 1979.

[12]Chen, R. T. N., "Effects of Primary Rotor Parameters on Flapping Dynamics," Tech. Rep. NTP 1431, NASA Ames Research Center, 1980.

[13]Boiffier, J. L., *The Dynamics of Flight The Equations*, John Wiley & Sons, Chichester, England, 1998.

[14]Misra, P. and Enge, P., *Global Positioning System: Signals, Measurements and Performance, Second Edition*, Ganga-Jamuna Press, Lincoln MA, USA, 2006.

[15]Padfield, G. D., *Helicopter Flight Dynamics*, Blackwell Science Ltd, Oxford, UK, 1996.

[16]Gessow, A. and Myers, G. C., *Aerodynamics of the Helicopter*, College Park Pr, 1999.

[17]Johnson, W., *Helicopter Theory*, Dover Publications Inc., NY, USA, 1994.

[18]Bramwell, A. R. S., *Bramwell's Helicopter Dynamics, Second Edition*, AIAA Inc., Reston VA, USA, 2001.

[19]Shevell, R. S., *Fundamentals of Flight*, Prentice Hall, Upper Saddle River NJ, 1989.

[20]Anderson, J. D., *Fundamentals of Aerodynamics. Third Ed.*, McGraw-Hill Higher Education, NY, 2001.

[21]Prouty, R. W., *Helicopter Performance, Stability, and Control*, Krieger Publishing Company, Malabar, Florida USA, 1995.

[22]Houck, J. A., Moore, F. L., Howlett, J. J., Pollock, K. S., and Browne, M. M., "Rotor Systems research Aircraft Simulation Mathematical Model," Tech. Rep. NTM 78629, NASA Langley Research Center, 1977.

[23]Pitt, D. M. and Peters, D. A., "Theoretical Prediction of Dynamic-Inflow Derivatives," *Vertica*, Vol. 5, 1981, pp. 21–34.

[24]Peters, D. A. and HaQuang, N., "Technical Notes - Dynamic Inflow for Practical Applications," *J. of the Am. Helicopter Soc.*, 1988, pp. 64–68.

[25]Peters, D. A. and He, C., "Technical Note: Modification of Mass-Flow parameter to Allow Smooth Transition Between Helicopter and Windmill States," *J. of the Am. Helicopter Soc.*, 2006, pp. 275–278.

[26]Leishman, G. J., *Principles of Helicopter Aerodynamics*, Cambridge University Press, Cambridge, UK, 2000.

[27]AviationToday, *Ask Ray Prouty: Gross Weights Effect on Autorotation*, Danbury CT ., U.S.A., 2007.

[28]Carlson, E. B., *Optimal Tiltrotor Aircraft Operations During Power Failure*, Ph.D. thesis, University of Minnesota, 1999.

[29]Aponso, B. L., Bachelder, E. N., and Lee, D., "Automated Autorotation for Unmanned Rotorcraft Recovery," *AHS Int. Specialists' Meeting On Unmanned Rotorcraft*, 2005.

[30]Fletcher, T. M. and Brown, R. E., "Main Rotor - Tail Rotor Wake Interaction and its Implications for Helicopter Directional Control," *Europ. Rotorcraft Forum*, 2006.

[31]Fletcher, T. M. and Brown, R. E., "Main rotor - tail rotor interaction and its implications for helicopter directional control," *J. of the Am. Helicopter Soc.*, Vol. 53, No. 2, 2008, pp. 125–138.

[32]Bailey, F. J., "A Simplified Theoretical Method of Determining the Characteristics of a Lifting Rotor in Forward Flight," Tech. Rep. RNo. 716, NACA, 1941.

[33]ART, *FLIGHTLAB Theory Manual (Vol. One & Two)*, Advanced Rotorcraft Technology, Inc., Mountain View CA, 2006.

[34]Voorsluijs, G. M., "A Modular Generic Helicopter Model," Tech. rep., Master Thesis, Delft University of Technology, 2002.

[35]Talbot, P. D., Tinling, B. E., Decker, W. A., and Chen, R. T. N., "A Mathematical Model of a Single Main Rotor Helicopter for Piloted Simulation," Tech. Rep. NTM 84281, NASA Ames Research Center, 1982.

[36]Jewel, J. W. and Heyson, H. H., "Charts of Induced Velocities Near a Lifting Rotor," Tech. Rep. 4-15-59LY, NASA, 1959.

[37]Gavrilets, V., Mettler, B., and Feron, E., "Nonlinear Model for a Small-Size Acrobatic Helicopter," *AIAA Guidance, Navigation and Control Conf.*, 2001.

[38]Pavel, M. D., *On the Necessary Degrees of Freedom for Helicopter and Wind Turbine Low-Frequency Mode-Modelling*, Ph.D. thesis, Delft University of Technology, 2001.

[39]Baskin, V. E., Vildgrube, L. S., Vozhdayev, Y. S., and Maykapar, C. I., "Theory of the Lifting Airscrew," Tech. Rep. TT-F-823, NASA, 1976.

[40]Zhao, X. and Curtiss, H. C., "A Study of helicopter Stability and Control Including Blade Dynamics," Tech. Rep. TR 1823T, NASA Ames Research Center, 1988.

[41]Takahashi, M. D., "A Flight-Dynamic Helicopter Mathematical Model with a Single Flap-Lag-Torsion Main Rotor," Tech. Rep. TM 102267, NASA Ames Research Center, 1990.

[42]Bertsekas, D., *Nonlinear Programming - Second Edition*, Athena Scientific, Belmont, MA, 1999.

[43]Nocedal, J. and Wright, S., *Numerical Optimization*, Springer, NY, 2000.

[44]Bazaraa, M. S., Sherali, H. D., and Shetty, C. M., *Nonlinear Programming: Theory and Algorithms - Third Edition*, Wiley-Interscience, 2006.

[45]Bliss, G. A., *Lectures on the Calculus of Variations*, University of Chicago Press, Chicago IL, 1946.

[46]Pontryagin, L. S., Boltyanskii, V. G., Gamkrelidze, R. V., Mishchenko, E. F., Trirogoff, K. N., and Neustadt, L. W., *Mathematical Theory of Optimal Processes*, Interscience, NY, 1962.

[47]Weinstock, R., *Calculus of Variations*, Dover Publications, NY, 1974.

[48]van Brunt, B., *The Calculus of Variations*, Springer-Verlag, NY, 2004.

[49]Gill, P. E., Murray, W., and Saunders, M. A., "SNOPT: An SQP Algorithm for Large-Scale Constrained Optimization," *SIAM Reviews*, Vol. 47, 2002, pp. 99–131.

[50]Gill, P. E., Murray, W., Saunders, M. A., and Wright, M. H., "Users Guide for SNOPT Version 7: Software for Large-Scale Nonlinear Programming," Tech. rep., University of California San Diego, 2008.

[51]SBS-Inc., http://www.sbsi-sol-optimize.com/asp/sol_product_snopt.htm, Stanford University, U.S.A.

[52]Vanderbei, R. J. and Shanno, D. F., "An Interior-Point Algorithm for Nonconvex Nonlinear Programming," *Computational Optimization and Applications*, Vol. 13, 1999, pp. 231–252.

[53]Byrd, R. H., Nocedal, J., and Waltz, R. A., "KNITRO: An Integrated Package for Nonlinear Optimization," *Large-Scale Nonlinear Optimization, Springer-Verlag*, 2006, pp. 35–59.

[54]Wachter, A., *An Interior Point Algorithm for Large-Scale Nonlinear Optimization with Applications in Process Engineering*, Ph.D. thesis, Carnegie-Mellon University, 2002.

[55]Wachter, A. and Biegler, L. T., "On the Implementation of an Interior-Point Filter Line-Search Algorithm for Large-Scale Nonlinear Programming," *Mathematical Programming*, Vol. 106, No. 1, 2006, pp. 25–57.

[56]Biegler, L. T. and Zavala, V. M., "Large-Scale Nonlinear Programming Using IPOPT: An Integrating Framework for Enterprise-Wide Optimization," *Computers and Chemical Engineering*, Vol. 33, 2008, pp. 575–582.

[57]Keller, H. B., "Numerical Solution of Two Point Boundary Value Problems," *SIAM*, 1976.

[58]Bock, H. G. and Plitt, K. J., "A Multiple Shooting Algorithm for Direct Solution of Optimal Control Problems," *IFAC 9th W.C.*, 1984.

[59]Stoer, J. and Bulirsch, R., *Introduction to Numerical Analysis*, Springer-Verlag, 2002.

[60]Reddien, G. W., "Collocation at Gauss Points as a Discretization in Optimal Control," *SIAM J. on Control and Optimization*, Vol. 17, No. 2, 1979, pp. 298306.

[61]Hargraves, C. R. and Paris, S. W., "Direct Trajectory Optimization Using Nonlinear Programming and Collocation," *AIAA J. of Guidance, Control, and Dynamics*, Vol. 10, No. 4, 1987.

[62]Enright, P. J. and Conway, B. A., "Discrete Approximations to Optimal Trajectories Using Direct Transcription and Nonlinear Programming," *AIAA J. of Guidance, Control, and Dynamics*, Vol. 15, No. 4, 1992.

[63]Hull, D., "Conversion of Optimal Control Problems into Parameter Optimization Problems," *AIAA J. of Guidance, Control, and Dynamics*, Vol. 20, No. 1, 1997, pp. 57–60.

[64]Biegler, L. T., "An Overview Of Simultaneous Strategies For Dynamic Optimization," *Chemical Engineering and Processing: Process Intensification*, Vol. 46, No. 11, 2007, pp. 1043–1053.

[65]Schwartz, A., *Theory and Implementation of Numerical Methods Based on Runge-Kutta Integration for Solving Optimal Control Problems*, Ph.D. thesis, University of California at Berkeley, 1996.

[66]Hager, W. W., "Runge-Kutta Methods in Optimal Control and the Transformed Adjoint System," *Numer. Math.*, Vol. 87, 2000, pp. 247282.

[67]Betts, J. T., "Practical Methods for Optimal Control Using Nonlinear Programming," *SIAM*, 2001.

[68]Kim, C. J., Sung, S. K., Park, S. H., Jung, S. N., and Yee, K., "Selection of Rotorcraft Models for Application to Optimal Control Problems," *AIAA J. of Guidance, Control, and Dynamics*, Vol. 31, No. 5, 2008.

[69]Betts, J. T., "Survey of Numerical Methods for Trajectory Optimization," *AIAA J. of Guidance, Control, and Dynamics*, Vol. 21, No. 2, 1998, pp. 193–207.

[70]Bottasso, C. L., Maisano, G., and Scorcelletti, F., "Trajectory Optimization Procedures for Rotorcraft Vehicles Including Pilot Models, with Applications to ADS-33 MTEs, Cat-A and Engine Off Landings," *Am. Helicopter Soc.*, 2009.

[71]Dickmanns, E. D. and Well, H., "Approximate Solution of Optimal Control Problems Using Third-Order Hermite Polynomial Functions," *6th Technical Conf. on Optimization Techniques*, 1975.

[72]Enright, P. J. and Conway, B. A., "Optimal Finite-Thrust Spacecraft Trajectories Using Collocation and Nonlinear Programming," *AIAA J. of Guidance, Control, and Dynamics*, Vol. 14, No. 5, 1991, pp. 981–985.

[73]Tang, S. and Conway, B., "Optimization of Low-Thrust Interplanetary Trajectories Using Collocation and Nonlinear Programming," *AIAA J. of Guidance, Control, and Dynamics*, Vol. 18, No. 3, 1995, pp. 599–604.

[74]Coverstone-Carroll, V. and Prussing, J. E., "Optimal Cooperative Power-Limited Rendezvous With Propellant Constraints," *J. of the Astronautical Sciences*, Vol. 43, No. 3, 1995, pp. 289–305.

[75]Herman, A. L. and Conway, B. A., "Direct Optimization Using Collocation Based on High-Order Gauss-Lobatto Quadrature Rules," *AIAA J. of Guidance, Control, and Dynamics*, Vol. 19, No. 3, 1996, pp. 592–599.

[76]Roh, W. and Kim, Y., "Trajectory Optimization for a Multi-Stage Launch Vehicle Using Time Finite Element and Direct Collocation Methods," *Engineering Optimization*, Vol. 34, No. 1, 2002, pp. 15–32.

[77]Hoffren, J. and Raivio, T., "Optimal Maneuvering After Engine Failure," *AIAA Atmospheric Flight Mechanics Conf.*, 2000.

[78]Hyde, D. C., "Minimum-Altitude-Loss Gliding Turns With Terminal Constraints (Return to Runway After Engine Failure)," *AIAA Atmospheric Flight Mechanics Conf.*, 2005.

[79]Brinkman, K. and Visser, H. G., "A closed-loop guidance approximation for the turn-back maneuver after engine failure during climb-out," *45th AIAA Aerospace Sciences Meeting and Exhibit*, 2007.

[80]Geiger, B. R., Horn, J. F., Sinsley, G. L., Ross, J. A., Long, L. N., and Niessner, A. F., "Flight Testing a Real-Time Direct Collocation Path Planner," *AIAA J. of Guidance, Control, and Dynamics*, Vol. 31, 2008, pp. 1575–1586.

[81]Bottasso, C. L., Chang, C. S., Croce, A., Leonello, D., and Riviello, L., "Adaptive Planning and Tracking of Trajectories for the Simulation of Maneuvers with Multibody Models," *Computer Methods in Applied Mechanics and Engineering*, 2006.

[82]Bottasso, C. L., Maisano, G., and Luraghi, F., "Efficient Rotorcraft Trajectory Optimization Using Comprehensive Vehicle Models by Improved Shooting Methods," *Europ. Rotorcraft Forum*, 2009.

[83]Bottasso, C. L., Maisano, G., and Scorcelletti, F., "Trajectory Optimization Procedures for Rotorcraft Vehicles, Their Software Implementation, and Applicability to Models of Increasing Complexity," *J. of the Am. Helicopter Soc.*, 2010.

[84]Misovec, K., Inanc, T., Wohletz, J., and Murray, R. M., "LowObservable Nonlinear Trajectory Generation for Unmanned Air Vehicles," *IEEE Conf. on Decision and Control*, 2003.

[85]Zhao, Y. J. and Qi, Y. C., "Minimum Fuel Powered Dynamic Soaring of Unmanned Aerial Vehicles Utilizing Wind Gradients," *Optimal Control Applications and Methods*, Vol. 25, No. 5, 2004, pp. 211233.

[86]Borrelli, F., Subramanian, D., Raghunathan, A. U., and Biegler, L. T., "MILP and NLP Techniques for Centralized Trajectory Planning of Multiple Unmanned Air Vehicles," *Am. Control Conf.*, 2006.

[87]Zhao, Y. J., "Optimal Patterns of Glider Dynamic Soaring," *Opt. Ctrl. App. and Meth.*, Vol. 25, No. 2, 2004, pp. 6789.

[88]Dontchev, A. L., Hager, W. W., and Veliov, V. M., "Second-Order Runge-Kutta Approximations In Constrained Optimal Control," *SIAM J. on Numerical Analysis*, Vol. 38, 2000, pp. 202226.

[89]Dontchev, A. L., Hager, W. W., and Veliov, V. M., "Uniform Convergence and Mesh independence of Newtons method for Discretized Variational Problems," *SIAM J. on Control and Optimization*, Vol. 39, 2000, pp. 961980.

[90]Cuthrell, J. E. and Biegler, L. T., "Simultaneous Optimization and Solution Methods for Batch Reactor Control Profiles," *Computers and Chemical Engineering*, Vol. 13, No. 12, 1989, pp. 4962.

[91]Kameswaran, S. and Biegler, L. T., "Convergence Rates for Direct Transcription of Optimal Control Problems at Radau Points," *Am. Control Conf.*, 2006.

[92]Elnagar, J., Kazemi, M. A., and Razzaghi, M., "The Pseudospectral Legendre Method for Discretizing Optimal Control Problems," *IEEE Trans. on Automatic Control*, Vol. 40, No. 10, 1995, pp. 17931796.

[93]Fahroo, F. and Ross, I. M., "Direct Trajectory Optimization by a Chebyshev Pseudospectral Method," *J. of Guidance, Control, and Dynamics*, Vol. 25, No. 1, 2002.

[94]Benson, D. A., *A Gauss Pseudospectral Transcription for Optimal Control*, Ph.D. thesis, Massachusetts Institute of Technology, 2004.

[95]Benson, D. A., Huntington, G. T., Thorvaldsen, T. P., and Rao, A. V., "Direct Trajectory Optimization and Costate Estimation via an Orthogonal Collocation Method," *AIAA J. of Guidance, Control, and Dynamics*, Vol. 29, No. 6, 2006.

[96]Huntington, G. T., *Advancement and Analysis of a Gauss Pseudospectral Transcription for Optimal Control*, Ph.D. thesis, Massachusetts Institute of Technology, 2007.

[97]Fahroo, F. and Ross, I. M., "Pseudospectral Methods for Infinite Horizon Nonlinear Optimal Control Problems," *AIAA Guidance, Navigation and Control Conf.*, 2005.

[98]Garg, D., Patterson, M. A., Darby, C. L., Francolin, C., Huntington, G. T., Hager, W. W., and Rao, A. V., "Direct Trajectory Optimization and Costate Estimation of General Optimal Control Problems Using a Radau Pseudospectral Method," *AIAA Guidance Navigation and Control Conf.*, 2009.

[99]Darby, C. L., Hager, W. W., and Rao, A. V., "Direct Trajectory Optimization Using a Variable Low-Order Adaptive Pseudospectral Method," *AIAA J. of Spacecraft and Rockets*, Vol. 48, No. 3, 2011.

[100]Ross, I. M. and Fahroo, F., "Pseudospectral Methods for Optimal Motion Planning of Differentially Flat Systems," *IEEE Trans. on Automatic Control*, Vol. 49, No. 8, 2004, pp. 1410–1413.

[101]Gong, Q., Kang, W., and Ross, I. M., "A Pseudospectral Method for the Optimal Control of Constrained Feedback Linearizable Systems," *IEEE Trans. on Automatic Control*, Vol. 51, No. 7, 2006.

[102]Rao, A. V., "A Survey of Numerical Methods for Optimal Control," *Am. Astronautical Soc.*, 2009.

[103]Fahroo, F. and Ross, I. M., "Second Look at Approximating Differential Inclusions," *AIAA J. of Guidance, Control, and Dynamics*, Vol. 24, No. 1, 2001.

[104]Fornberg, B., *A Practical Guide to Pseudospectral Methods*, Cambridge University Press, 1998.

[105]Dai, R. and Cochran, J. E., "Wavelet Collocation Method for Optimal Control Problems," *J. Optim. Theory Appl.*, Vol. 143, 2009, pp. 265278.

[106]Davis, P. J. and Rabinowitz, P., *Methods of Numerical Integration*, Dover Publications, 2007.

[107]Vlassenbroeck, J. and Doreen, R. V., "Chebyshev Technique for Solving Nonlinear Optimal Control Problems," *IEEE Trans. on Automatic Control*, Vol. 33, No. 4, 1988, pp. 333340.

[108]Huntington, G. T., Benson, D. A., and Rao, A. V., "A Comparison of Accuracy and Computational Efficiency of Three Pseudospectral Methods," *AIAA Guidance, Navigation, and Control Conf.*, 2007.

[109]Gottlieb, D., Hussaini, M. Y., and Orszag, S. A., "Theory and Applications of Spectral Methods," *SpectralMethods for PDEs. Soc. of Industrial and Applied Mathematics (SIAM)*, 1984.

[110]Canuto, C., Hussaini, M. Y., Quarteroni, A., and Zang, T. A., *Spectral Methods in Fluid Dynamics*, Springer-Verlag, New York, 1988.

[111]Neuman, C. P. and Sen, A., "A Suboptimal Control Algorithm for Constrained Problems using Cubic Splines," *Automatica*, Vol. 9, 1973, pp. 601–613.

[112]Lu, P., Sun, H., and Tsai, B., "Closed-Loop Endoatmospheric Ascent Guidance," *AIAA J. of Guidance, Control and Dynamics*, Vol. 26, No. 2, 2003, pp. 283–294.

[113]Rea, J., "Launch Vehicle Trajectory Optimization Using a Legendre Pseudospectral Method," *AIAA Guidance, Navigation, and Control Conf.*, 2003.

[114]Josselyn, S. and Ross, I. M., "Rapid Verification Method for the Trajectory Optimization of Reentry Vehicles," *AIAA J. of Guidance, Control, and Dynamics*, Vol. 26, No. 3, 2003.

[115]Williams, P., "Application of Pseudospectral Methods for Receding Horizon Control," *AIAA J. of Guidance, Control, and Dynamics*, Vol. 27, No. 2, 2004, pp. 310–314.

[116]Infeld, S. I., *Optimization of Mission Design for Constrained Libration Point Space Missions*, Ph.D. thesis, Stanford University, 2005.

[117]Riehl, J. P., Paris, S. W., and Sjaw, W. K., "Comparision of Implicit Integration Methods for Solving Aerospace Trajectory Optimization Problems," *AIAA/AAS Astrodynamics Specialists Conf.*, 2006.

[118]Hawkins, A. M., Fill, T. R., Proulx, R. J., and Feron, E. M., "Constrained Trajectory Optimization for Lunar Landing," *AAS Spaceflight Mechanics Meeting*, 2006.

[119]Bollino, K. P., Lewis, L. R., Sekhavat, P., and Ross, I. M., "Pseudospectral Optimal Control: A Clear Road for Autonomous Intelligent Path Planning," *AIAA Infotech*, 2007.

[120]Bedrossian, N., Bhatt, S., Lammers, M., Nguyen, L., and Zhang, Y., "First Ever Flight Demonstration of Zero Propellant Maneuver TM Attitude Control Concept," *AIAA Guidance, Navigation, and Control Conf.*, 2007.

[121]Gong, Q., Wei, K., Bedrossian, N. S., Fahroo, F., Sekhavat, P., and Bollino, K., "Pseudospectral Optimal Control for Military and Industrial Applications," *IEEE Conf. on Decision and Control*, 2007.

[122]Ross, I. M., Sekhavat, P., Fleming, A., and Gong, Q., "Optimal Feedback Control: Foundations, Examples, and Experimental Results for a New Approach," *AIAA J. of Guidance, Control, and Dynamics*, Vol. 31, No. 2, 2008.

[123]Karpenko, M., Bhatt, S., Bedrossian, N., Fleming, A., and Ross, I. M., "Flight Implementation of Pseudospectral Optimal Control for the TRACE Space Telescope," *AIAA Guidance, Navigation and Control Conf.*, 2011.

[124]Ceriotti, M. and McInnes, C. R., "Generation of Optimal Trajectories for Earth Hybrid Pole Sitters," *AIAA J. of Guidance, Control, and Dynamics*, Vol. 34, No. 3, 2011, pp. 847–859.

[125]Yan, H., Gong, Q., Park, C. D., Ross, I. M., and Souza, C. N. D., "High-Accuracy Trajectory Optimization for a Trans-Earth Lunar Mission," *AIAA J. of Guidance, Control, and Dynamics*, Vol. 34, No. 4, 2011, pp. 1219–1227.

[126]Darby, C. L. and Rao, A. V., "Minimum-Fuel Low-Earth-Orbit Aeroassisted Orbital Transfer of Small Spacecraft," *AIAA J. of Spacecraft and Rockets*, Vol. 48, No. 4, 2011.

[127]Boyarko, G., Yakimenko, O., and Romano, M., "Optimal Rendezvous Trajectories of a Controlled Spacecraft and a Tumbling Object," *AIAA J. of Guidance, Control, and Dynamics*, Vol. 34, No. 4, 2011, pp. 1239–1252.

[128]Boyarko, G., Romano, M., and Yakimenko, O., "Time-Optimal Reorientation of a Spacecraft Using an Inverse Dynamics Optimization Method," *AIAA J. of Guidance, Control, and Dynamics*, Vol. 34, No. 4, 2011, pp. 1197–1208.

[129]Zhang, K. and Chen, W., "Reentry Vehicle Constrained Trajectory Optimization," *AIAA Int. Space Planes and Hypersonic Systems and Technologies*, 2011.

[130]Paris, S. W., Riehl, J. P., and Sjaw, W. K., "Enhanced Procedures for Direct Trajectory Optimization Using Nonlinear Programming and Implicit Integration," *AIAA/AAS Astrodynamics Specialists Conf.*, 2006.

[131]Cottrill, G. C. and Harmon, F. G., "Hybrid Gauss Pseudospectral and Generalized Polynomial Chaos Algorithm to Solve Stochastic Trajectory Optimization Problems," *AIAA Guidance Navigation and Control Conf.*, 2011.

[132]Dekel, M. and Ben-Asher, J. Z., "Pseudo-Spectral-Method Based Optimal Glide in the Event of Engine Cut-off," *AIAA Guidance, Navigation, and Control Conf.*, 2011.

[133]Dai, R. and Cochran, J. E., "Three-Dimensional Trajectory Optimization in Constrained Airspace," *AIAA J. of Aircraft*, Vol. 46, No. 2, 2009, pp. 627634.

[134]Hartjes, S., Visser, H. G., and Pavel, M. D., "Environmental Optimization Of Rotorcraft Approach Trajectories," *Europ. Rotorcraft Forum*, 2011.

[135]Harada, M. and Bollino, K., "Optimal Trajectory of a Glider in Ground Effect and Wind Shear," *AIAA Guidance, Navigation and Control Conf.*, 2005.

[136]Gong, Q., Lewis, L. R., and Ross, I. M., "Pseudospectral Motion Planning for Autonomous Vehicles," *AIAA J. of Guidance, Control, and Dynamics*, Vol. 32, No. 3, 2009.

[137]McCracken, B. D., Burzota, K. L., Ramos, M. M., and Jorris, T. R., "Cooperative Unmanned Air Vehicle Mission Planning and Collision Avoidance," *AIAA Infotech*, 2011.

[138]Choe, R. and Hovakimyan, N., "Perching Maneuver for an MAV Augmented with an L1 Adaptive Controller," *AIAA Guidance, Navigation, and Control Conf.*, 2011.

[139]la Cour-Harbo, A. and Bisgaard, M., "State-Control Trajectory Generation for Helicopter Slung Load System using Optimal Control," *AIAA Guidance, Navigation, and Control Conf.*, 2009.

[140]Harada, M. and Bollino, K., "Minimum-Time Circling Flight of a Triarm Coaxial Rotor UAV," *AIAA Guidance Navigation and Control Conf.*, 2011.

[141]Hornik, K., Stinchcombe, M., and White, H., "Multilayer Feedforward Networks are Universal Approximators," *Neural Networks*, Vol. 2, 1989, pp. 359–366.

[142]Norgaard, M., Ravn, O., Poulsen, N., and Hansen, L., *Neural Networks for Modelling and Control of Dynamic Systems*, Springer-Verlag, London, 2000.